Bimetallic Catalysts For Sustainable Chemistry: Surface Redox Reactions For Tuning The Catalytic Surface Composition

Catherine Especel, Gwendoline Lafaye, Florence Epron

Accepted manuscript

Bimetallic Catalysts For Sustainable Chemistry: Surface Redox Reactions For Tuning The Catalytic Surface Composition

MINIREVIEW

Catherine Especel, Gwendoline Lafaye and Florence Epron*

In memory of Daniel Duprez

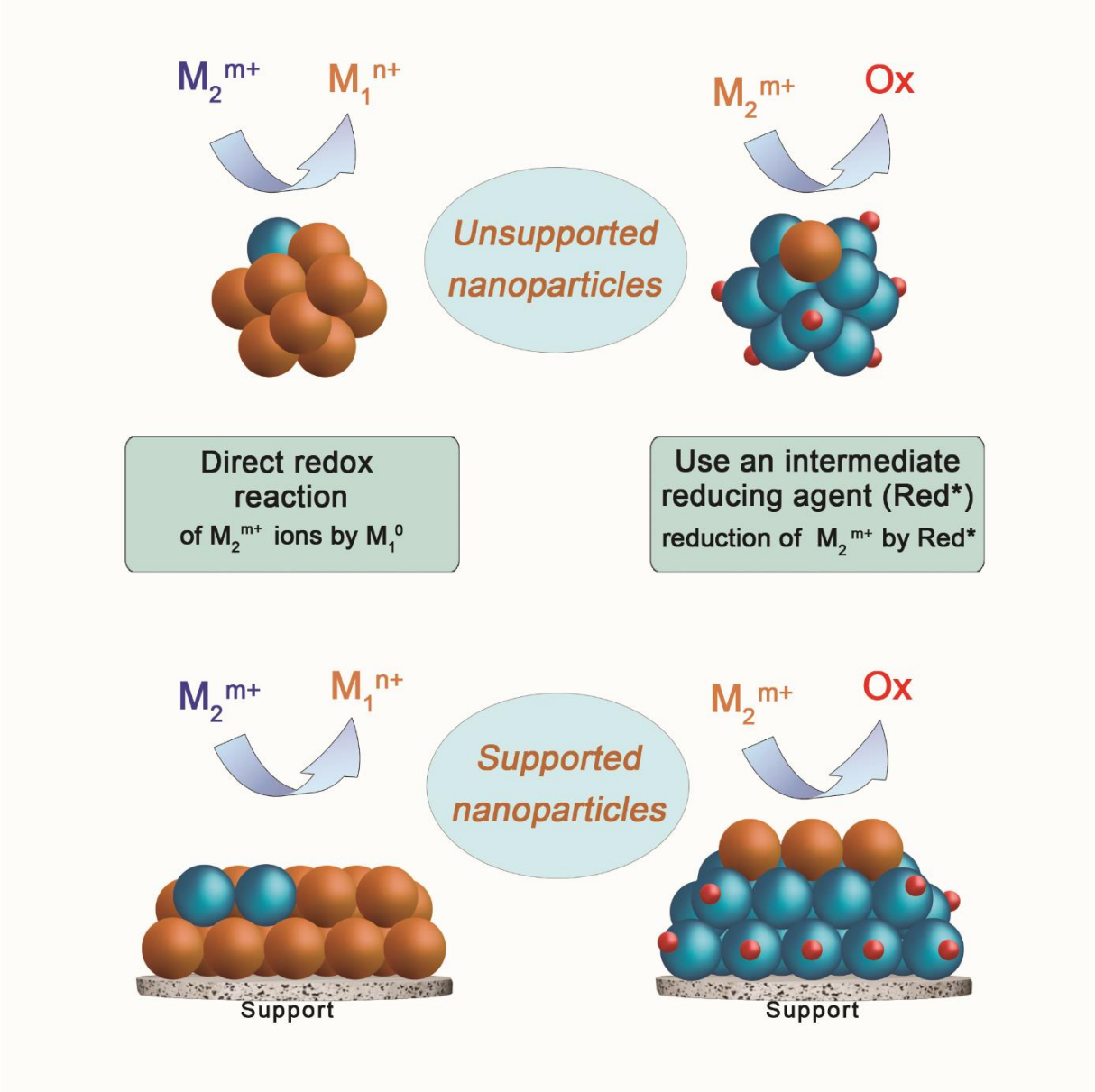

Bimetallic Catalysts For Sustainable Chemistry: Surface Redox Reactions For Tuning The Catalytic Surface Composition

MINIREVIEW

Prof. Dr. Catherine Especel, Dr. Gwendoline Lafaye and Dr. Florence Epron*

In memory of Daniel Duprez

Institut de Chimie des Milieux et Matériaux de Poitiers (IC2MP), CNRS, Université de Poitiers, F-86073 Poitiers, France

*Corresponding author : florence.epron@univ-poitiers.fr

ToC graphic:

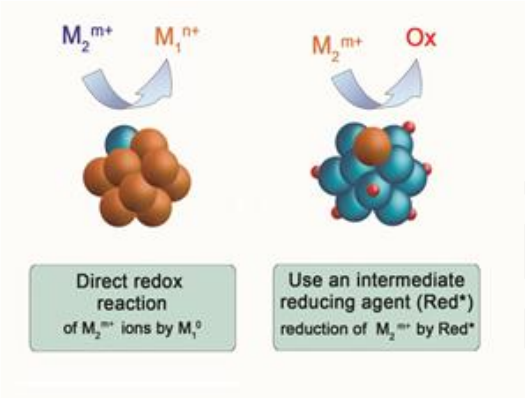

This minireview describes the fundamental bases of the preparation of supported or unsupported bimetallic catalysts by redox reactions and the recent advances in that domain. These preparation methods enable the deposition of a second metal at the surface of monometallic nanoparticles, leading to bimetallic nanoparticles with strong metal-metal interactions and enhanced catalytic properties compared to their monometallic counterparts.

Catherine Especel is Full Professor at the Institute of Chemistry Materials and Natural Resources of Poitiers (IC2MP), University of Poitiers, France. Her research's group SAMCat focuses on the design of catalytic and electrocatalytic materials for applications mainly in the fields of energy and environement. Her main research topics include the preparation of multimetallic catalysts notably by using surface redox reactions, with applications in fine chemistry, biomass valorisation and energy: selective hydrogenation of α,β-unsaturated aldehydes and carboxylic acids, hydrogenolysis of polyols, catalytic reforming, selective ring opening of naphtenic cycles, dehydrogenation of alkanes).

Gwendoline Lafaye is an Associate Professor at the Institute of Chemistry Materials and Natural Resources of Poitiers (IC2MP), University of Poitiers, France. Her main scientific interests are the preparation of heterogeneous catalysts and the investigation of the structure-activity relationship of these materials. Targeted applications include abatement of organic compounds in water by catalytic wet air oxidation and selective hydrogenation of unsaturated compounds such as unsaturated aldehydes towards valuable products

Florence Epron obtained her PhD in Chemistry of Materials at the University Pierre et Marie Curie (Paris) in 1991. After a post-doc, she joined the Centre National de la Recherche Scientifique (CNRS) in 1994 as a permanent researcher in the Laboratoire de Catalyse en Chimie Organique at the University of Poitiers. She is now Research Director at CNRS and Deputy director of the Institute of Chemistry Materials and Natural Resources of Poitiers (IC2MP). After having focused her research work in the development of monometallic and bimetallic catalysts for water treatment, mainly for nitrate reduction, she extended her skills to hydro/dehydrogenation reactions for application in the domain of energy, such as hydrogen production and biogas valorization.

Abstract

The development of a bimetallic catalyst for a given reaction requires not only the selection of the appropriate metals M_1 and M_2 but also the control as far as possible of the distribution of the two metals together and at the support surface in the case of supported catalysts. Preparation methods using redox reactions specifically enable the deposition of a second metal M_2 at the surface of monometallic M_1 nanoparticles, leading in most cases to core-shell nanoparticles with strong metal-metal interactions. Various methods are possible depending on the electrochemical potentials of the species involved: either a direct redox reaction, also named galvanic replacement, or the reduction of an intermediate reducing agent activated at the surface of M_1. In this minireview, the fundamental bases of the preparation of bimetallic catalysts by both types of redox reactions and the recent advances in that domain are described.

Key-words: metal-metal interaction, bimetallic catalysts, redox chemistry, galvanic replacement, electroless deposition.

Introduction

Since the first publications highlighting the use of bimetallic systems in heterogeneous catalysis dating back to 1950 [1-3], the interest of combining two elements to design catalysts with specific properties has continued to grow over the years. In the first articles published in the field, the catalytic behavior of these alloys was explained exclusively in terms of electronic effects, based on the so-called “rigid band theory” according to which, when going from left to right in the periodic table, the “rigid” band of energy levels of the valence electrons is successively filled by electrons.[4] The catalytic activation of adsorbed molecules was then considered to be govern by both incompletely filled d-bands and a high density of states at the Fermi level for a given active metal, these conditions being the most optimal for electron transfer. Thus, according to this theory, a bimetallic system was considered as composed of another metal in which the two initial components are no more distinguishable. As opposed to this “collective” model, other scientists supported the idea that properties of the individual metal atoms are preserved in bimetallic catalysts, and demonstrated by titration with chemisorbed hydrogen that the bond strength between the adsorbing atom and the adsorbate can be modified by the direct neighbors in and below the surface, giving rise to the ensemble or ligand effect.[5] The best achievements in catalysis brought by alloying two metals can be found in the refining industry with the very famous reforming Pt-Re systems [6] or in petrochemistry with Pt-Sn catalysts for selective hydrogenations or hydrogenolysis [7,8] for instance.

By combining two different metals, researchers tried to prepare bimetallic formulations able to exhibit catalytic performance (*i.e.* activity and/or selectivity and/or stability) higher than those displayed by both monometallic catalysts working individually, that is to say a synergetic effect resulting from metal-metal interactions generated within bimetallic entities with varied morphologies (alloys, Janus-type particles, core-shell systems, etc.). The combination can concern two active metals, an inactive with an active one (like the Pt-Sn systems previously mentioned), or two inactive ones whose association will lead to the appearance of catalytic performance (as Au-Ni systems, for example, demonstrating a strong synergetic effect for allylbenzene isomerization [9]).

Many chemical methods were developed for synthesizing bimetallic catalysts allowing one to control more or less precisely the formation of bimetallic interactions. For the supported catalysts, the most conventional syntheses are performed by impregnation of the precursors salts on the support, simultaneously (coimpregnation) or successively (successive impregnation), or by deposition-precipitation, with the drawback to hardly controlling the final composition of the nanoparticles and then of the presence of bimetallic interaction [10]. Less conventional methods as those using microemulsion or microsuspension processes can be considered more suitable for generating bimetallic entities, but they have the disadvantage to

use polymers as templating agents, which are generally difficult to remove during catalyst preparation.

In this context, surface redox reactions were developed in the 1990s by Barbier's group in Poitiers (France) [11-17], for synthesizing bimetallic supported catalysts with controlled metal-metal interaction. The preparation of bimetallic M_1-M_2 catalysts by surface redox reactions occurs between atoms in the reduced state at the surface of the monometallic M_1 nanoparticles and the oxidized form of the M_2 modifier in solution. It is governed by the electrochemical potential of the species implied in the reaction. This process can be direct (direct redox reaction with M_1) or may involve an intermediate reducing agent activated at the surface of M_1, as H_2, for reducing the oxidized form of the M_2 modifier (refilling or catalytic reduction) or other reducing agents (electroless deposition). The main goal of this minireview is to draw up an inventory of the most recent work dealing with the use of these different redox processes to prepare bimetallic nanoparticles, supported or not supported.

1. Direct redox reactions

1.1. Generalities

Among the surface redox reactions, the so-called "direct redox" (DR) method, also named "galvanic replacement (GR) or displacement", is the electrochemical process that involves the oxidation of one metal (which is referred to the parent metal M_1 which is sacrificed (corroded)) by the ions of another metal having a higher reduction potential (considered as the modifier or promoter metal M_2). The direct redox process is driven by the favorable difference in reduction potential between the two elements considered to lead to the following redox reaction (1):

$$m\ M_1 + n\ M_2^{m+} \rightarrow m\ M_1^{n+} + n\ M_2 \quad (1)$$

The reaction (1) will be spontaneous if its Gibbs free energy (ΔG) is negative, the value of ΔG being determined by equation (2):

$$\Delta G = - zF\Delta E \quad (2)$$

where z is the number of electrons transferred in the half redox reaction, F is Faraday's constant and ΔE is the potential difference between the involved electrochemical half reactions calculated using the Nernst equation given in equation (3) (established below for the M_1^{n+}/M_1 redox couple).

$$E_1 = E_1° + \frac{RT}{nF} \ln \frac{a_{M1^{n+}}}{a_{M1}} \quad (3)$$

where $a_{M1^{n+}}$ and a_{M1} are the activities of oxidized (M_1^{n+}) and reduced (M_1) species, respectively, $E_1°$ is the standard reduction potential at 25 °C, R is the gas constant and T is the temperature.

The system reach the equilibrium when the two half-reactions E_1 and E_2 are equal with the same number of electrons exchanged in the two half reactions.

According to reaction (1), the direct redox reaction leads to the replacement of surface atoms of the M_1 metallic particles by atoms M_2 of the modifier. An illustration is given in Figure 1 in the case of a macroscopic object corresponding to a Cu wire immersed in an aqueous $AgNO_3$ solution, showing after 10 min the noticeable quantity of release blue Cu^{2+} ions in solution and the grey deposit of Ag atoms on the surface of the Cu wire [18]. The galvanic replacement reaction can be facilitated by introducing ionic species in the medium, such as halides, that can change the reduction potential of the metal/ion pairs by complexation effect, thus shifting the thermodynamic equilibrium, as well as modifying the reaction kinetics [18]. A wide variety of M_1M_2 nanoparticles, supported or not supported, can be generated by this type of reaction which represents a facile and versatile route to tune the elemental compositions of the final catalysts (by adjusting the amount of added modifier precursor salts), as well as the morphology of the synthesised multifunctional nanostructures (the redox process occurring generally on specific sites of the parent metal M_1) [19-24]. The M_2 metal involved as modifier in the studies based on direct reaction process is generally a noble metal (Au, Pt, Pd, Ag, Rh…) displaying high values of standard reduction potential relative to the standard hydrogen electrode. Knowledge of the experimental conditions (temperature, oxidation state and concentrations of relevant ions notably) can also affect these values and modulate the direction of the replacement reaction [25,26].

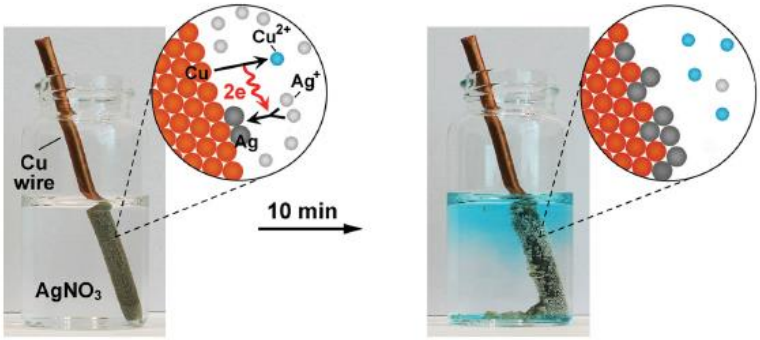

Figure 1. Direct rec reaction between Cu atoms of a Cu wire and Ag^+ ions of an $AgNO_3$ solution. Adapted with permission from Ref. [18]. Copyright © 2013 John Wiley and Sons.

1.2. Direct redox reaction over monometallic nanoparticles

Direct redox reactions are now commonly used to synthesize hollow nanomaterials displaying high surface-to-volume ratio and effective mass transport of reactants compared to their solid counterparts, thus generating excellent materials for many technological applications such as

catalysis [27-30]. An example is illustrated in Figure 2 for a Ag nanoparticle undergoing a galvanic replacement reaction with a $HAuCl_4$ solution [18], with 1) an immediate replacement of three Ag atoms located on sites with the highest surface energy (defect or steps for instance) by one Au atom which is deposited epitaxially on the surface (the crystal structure and the lattice constant of both metal being comparable), generating a small hole on the surface of the nanoparticle, opening the way to all the species involved in the reaction to diffuse in and out of the cavity and then 2) allowing the formation of an alloy that can turn to 3) a hollow interior and alloyed shell. This particular hollow structure will be disintegrated if the addition of Au^{3+} ions proceeds causing 4) dealloying by selective removing of Ag atoms from the Ag-Au shells, which can lead at the end 5) to the formation of small clusters of pure Au. It can be noticed that the dealloying process can also be favoured by using an external wet etchant such as NH_4OH for instance [18]. The combination of galvanic replacement and dealloying process was recently used by Yan *et al.* as a facile route to synthesize porous hollow Au nanoshells from Ag nanoparticles, with excellent catalytic properties towards the reduction of *p*-nitrophenol by $NaBH_4$ [31]. When small quantities of modifier are introduced, the galvanic replacement can occur on specific sites of the host nanoparticles, as illustrated by Zhang *et al.* who modified Pd nanosheets exclusively at edges with Au nanoparticles. These catalysts tested in the carbonylation of iodobenzene by carbon monoxide demonstrated an increase in the iodobenzene conversion by a factor of 25 and a similar selectivity towards ethylbenzoate compared to bare Pd nanosheets, while Au nanoparticles were inactive for this reaction [32].

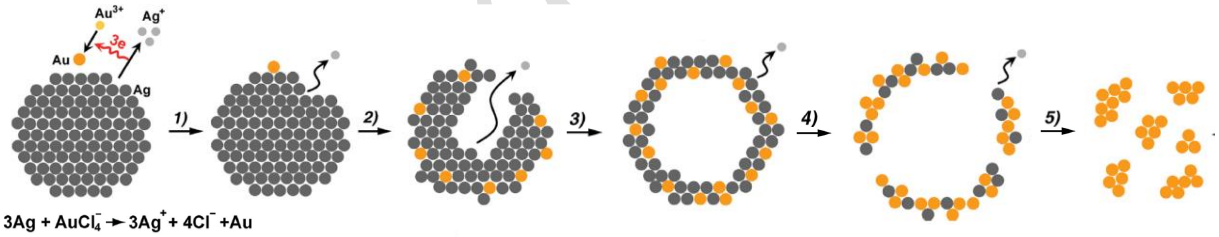

Figure 2. Schema of the morphological and structural changes at different stages of the GR reaction between a Ag particle and a $HAuCl_4$ aqueous solution. Adapted with permission from Ref. [18]. Copyright © 2013 John Wiley and Sons.

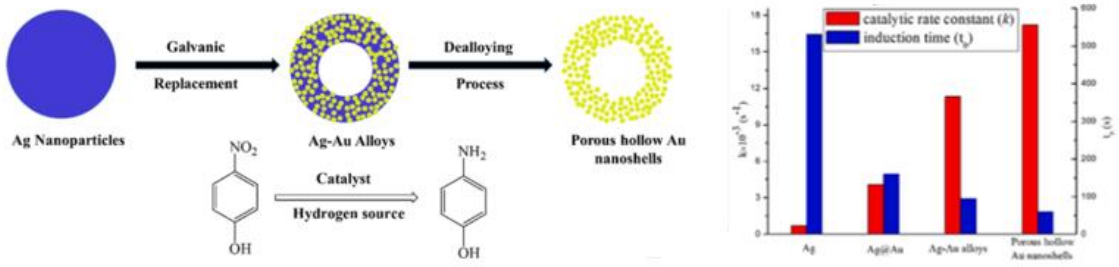

Figure 3. Schematic illustration of the synthesis by GR reaction followed by dealloying process of porous hollow Au nanoshells highly performant for reduction of *p*-nitrophenol. Adapted with permission from Ref. [31]. Copyright © 2020 Elsevier.

In situ characterization technics by optical spectroscopy and electron microscopy have revealed that the mechanism of the formation of these hollow structures can be more complex, involving Kirkendall effects due to unequal diffusion rates between the metal atoms notably at higher temperatures [33,34]. By using *in-situ* liquid cell transmission electron microscopy (TEM), Chee *et al.* evidenced that the Kirkendall effect occurs in conjunction with the galvanic replacement reaction between Ag nanocubes and Au ions [35]. When the GR is performed at 90 °C (Figure 4), at 9.6 s reaction time, two Kirkendall voids appear at the interface between the inner shell and the Ag nanocube, growing further until forming a nanobox at 17.6 s reaction time. The formation and growth of these voids was attributed to a concentration gradient causing the diffusion of Ag atoms into and through the Au layer, knowing that the diffusion of Ag into Au is faster that the diffusion of Au into Ag. Moreover, the synergistic combination of a galvanic replacement reaction, the Kirkendall effect and an etching reaction allowed Zhao *et al.* to synthesize a special type of core-shell structure, named yolk-shell, corresponding to a core@void@shell configuration from Ni spheres dispersed in a $SnCl_2$ solution [36].

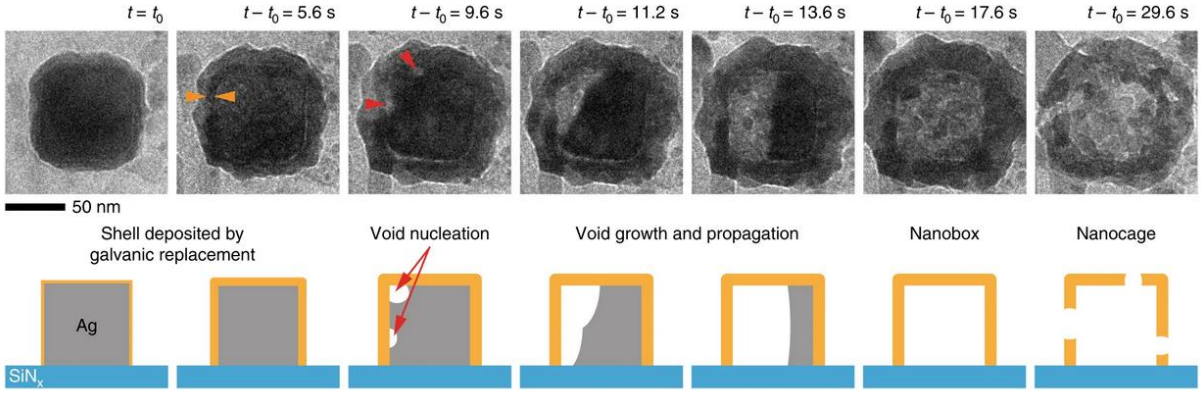

Figure 4. *In situ* TEM images and corresponding schematic representations showing the morphological evolution as function of the GR reaction time between a Ag nanocube and Au solution at 90 °C (SiN_x: silicon nitride membrane window; orange arrows: inner shell with darker contrast corresponding to the Au layer; red arrows: observed void nucleation). Adapted from Ref. [35].

With the ability to prepare metal nanocrystals of controlled shapes and sizes, their transformation by GR approach can then generate advanced catalysts by controlling the formation of hollow interior and shell thickness, with active sites embedded inside the hollow nanostructures, which improves their stability against aggregation or sintering [37,38]. Zeng *et al.* has demonstrated that the catalytic properties of Au-based catalysts prepared by galvanic replacement of Ag nanocubes are directly linked to the type of formed hollow nanostructures [39]. The authors prepared three different Au-Ag nanostructures, *i.e.* Au nanocages and Au nanoboxes with a complete hollow interior (with an average wall thickness of 5 and 6 nm, respectively), and partially hollow nanoboxes with a significant amount of unreacted Ag remaining inside (with wall thickness around 13 nm), that they compared to solid Au nanoparticles of same size (50 nm) or smaller (5 nm). For the model reaction based on the

reduction of *p*-nitrophenol by $NaBH_4$, they observed the Au nanocages with the most porous morphology and the thinnest wall displayed the highest reaction rate constant (10 times higher than the value obtained for Au nanoparticles of same size). Slater *et al.* have also correlated the 3D structure of Ag-Au nanoparticles obtained by the galvanic replacement reaction and their catalytic activity displayed for the three-component coupling reaction among cyclohexanecarboxyaldehyde, piperidine and phenylacetylene to produce propargylamines (Figure 5A) [40]. By varying the amount of $AuCl_4^-$ metal salts in the course of GR process, they prepared AgAu bimetallic nanoparticles with controlled compositions and shapes (solids *vs* hollow interiors), and determined by STEM imaging with EDX spectroscopy the exact elemental distribution of each metal with an excellent spatial resolution (Figure 5C). They identified that the direct redox reaction initiates with the formation of a gold surface layer at a low Au concentration (Figure 5Ca), which immediately transforms into an hollow Au−Ag alloy with the increase of the Au content because of the fast interdiffusion between gold and silver (Figure 5Cb and Figure 5Cc), evolving finally towards a reversal in the surface segregation by a dealloying effect (such as Ostwald ripening) leading to nanoparticles with a silver surface (Figure 5Cd). Higher yields of propargylamine were observed for all the hollow AgAu nanoparticles compared to the solid and monometallic systems with a maximum at 18 at. % Au (Figure 5B), corresponding to the point at which the particles change from Au surface segregation to a homogeneously alloyed composition.

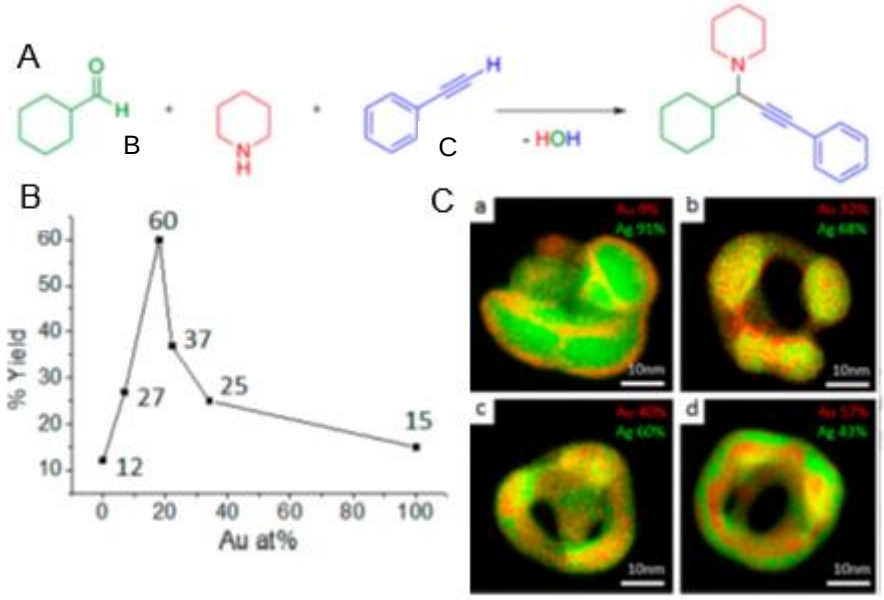

Figure 5. (A) Three-component coupling reaction to form propargylamines. (B) Propargylamine yield after 12 h reaction time at 90 °C as a function of the composition of the Ag-Au nanoparticles. (C) STEM EDX mapping showing the inversion of surface segregation behavior for Ag-Au nanoparticles as the Au content is increased, with EDX maps of representative nanoparticles of each studied stoichiometry: (a) $Ag_{93}Au_7$, (b) $Ag_{82}Au_{18}$, (c) $Ag_{78}Au_{22}$ and (d) $Ag_{66}Au_{34}$. Adapted from Ref. [40].

Camargo's group has demonstrated that varying the reaction temperature during the synthesis of bimetallic nanoparticles by galvanic replacement can tune their morphology and surface segregation, because influencing the redox reaction, the possibility of alloying or diffusion rate [10]. An example concerns the AgPt system obtained from GR between Ag nanowire and $PtCl_6^{2-}$ solution performed either at 100 °C or ambient temperature (Figure 6). At room temperature, the Ag ions formed during the redox process precipitate as AgCl crystals at the surface of the Ag nanowire, acting further as templates for the Pt deposition, inducing a growth in an island-mode and limiting the surface diffusion, whereas at 100 °C no precipitation occurs keeping the smooth surface of Ag nanowires as templates. This example illustrates how the temperature of the redox reaction may affect the way the second metal is deposited by GR.

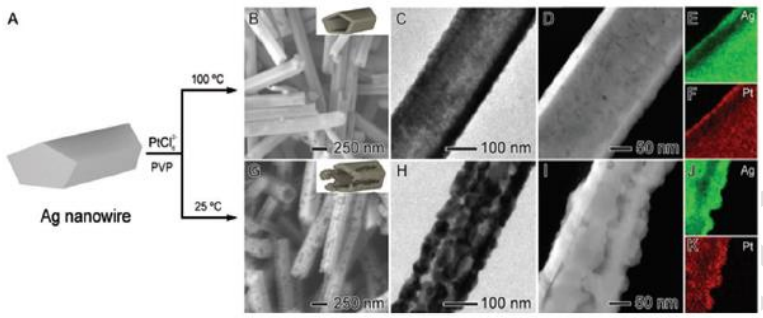

Figure 6. (A) Galvanic replacement between Ag nanowires and $PtCl_6^{2-}$ ions performed either at 100 °C or room temperature leading respectively to the formation of smooth (B-F) or rough (G-K) surfaces, as illustrated on the SEM (B, G), HRTEM (C, H), STEM HAADF (D, I,), STEM EDX (E, F, J, K) images. Adapted with permission from Ref. [10]. Copyright © 1996 Royal Society of Chemistry.

Conversely, Wang *et al.* operated a galvanic replacement reaction for the first time at ultralow temperatures below 0 °C (between - 20 and - 60 °C). By replacing some Fe atoms of an iron sheet by Au, they synthesize Au/Fe sheets with atomically dispersed Au nanoparticles, exhibiting high catalytic activity for methanol electro-oxidation and excellent stability [41]. With a lower reaction temperature, they observed that the synthesized Au nanoparticles are smaller, inducing a synergistic effect with Fe.

Other interesting approaches involving the galvanic replacement reaction were also studied as the synthesis of trimetallic nanomaterials [42-45] with controlled compositions by adjusting the molar ratio between the sacrificial templates and the metal modifier solutions introduced sequentially, or the coupling with co-reducing agents to provide a significant control over morphology for instance [39,46]. In the course of the galvanic replacement of Ag by Au in presence of ascorbic acid as co-reducing agent, Yang *et al.* have observed that the freed Ag^+ ions are immediately reduced and deposited back onto the surface of the template leading to alloyed AgAu nanocages with more that 80 % of the initial Ag content retained in the walls [47]. The influence of the presence of a surfactant was also evaluated in the course of the

preparation of AgPt bimetallic nanoparticles by direct redox reaction, revealing its passivating effect of the surface of the Ag nanoparticles templates as well as its stabilizing role of the Pt ions by the formation of complexes [48].

Figure 7 shows that the use of the PVP surfactant leads to smooth surface structures with a controllable thickness (notably with the use of mineral acids) evolving towards nanocages after dealloying of the Pt shells, compared to a growth of Pt onto Ag in an island-mode without surfactant as a consequence of the Pt-Ag immiscibility.

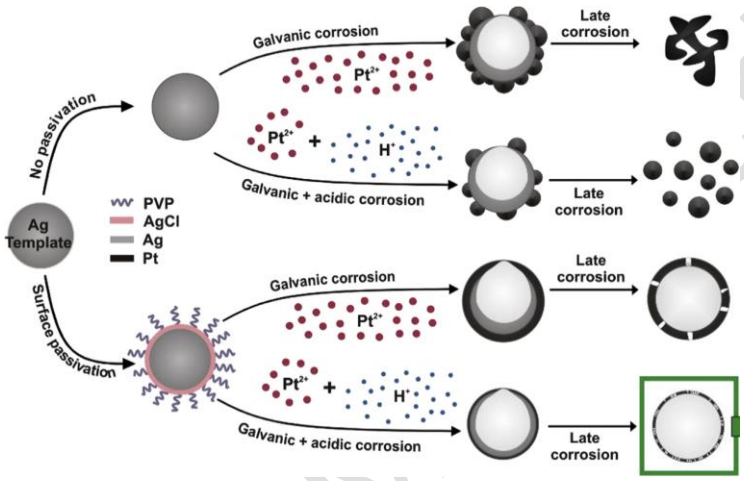

Figure 7. Schematic representation of distinct types of AgPt hollow nanoparticles obtained by galvanic replacement performed in various conditions (PVP: polyvinylpyrrolidone). Adapted with permission from Ref. [48]. Copyright © 2020 Elsevier.

Carbon monoxide was also used as a stabilizing and/or reducing agent in the course of the synthesis of Co-Pt electrocatalysts *via* the reaction of a Pt salt with Co nanoparticles prepared by thermal decomposition of a Co carbonyl precursor, the CO species being generated from this decomposition step [49]. More generally, the galvanic replacement method has been widely used for several years to prepare bimetallic electrode materials, such as (i) Pt-Pd, Pt-Ni or Pt-Ag alloy, for instance, for the oxygen reduction reaction (ORR) in proton exchange membrane fuel cells (PEMFCs) or methanol fuel cells [18,50,51], (ii) Pt-Co, Pt-Ni, Pt-Cu, Pd-Ni or Ag-Au electrocatalysts for alcohol oxidation [52-55], (iii) Ir-Co core-shell systems, Pd-Sn hollow alloys or Pt-Pd nanoparticles for the production of H_2 through water splitting reaction [56-58].

In conclusion, the choice of the M_1-M_2 couple and the experimental conditions applied during the synthesis of bimetallic systems by galvanic replacement are determinant parameters on the morphology of the as-obtained nanoparticles. The outermost electronic configurations and atomic radius of both metals remain crucial factors, as emphasized by Wang *et al.* [59] who prepared series of bimetallic systems M_2(Pt, Pd, Cu, Ag, Au)-M_1(Co, Ni, Cu) by GR starting from $M_1 = Co^0$, Ni^0 and Cu^0. They observed three types of states: (i) ad-metal atoms monolayer

dispersed on the surface of sub-metal for Pt(Pd, Cu)-Co(Ni), (ii) ad-metal atoms forming solid solution with surface sub-metal atoms for Pt(Pd, Au)-Cu, and (iii) ad-metal atoms with no interaction with sub-metal as in the simple mixture of respective crystallites for Ag(Au)-Co(Ni) and Ag-Cu. Thus, for instance, similar states were obtained for Co- and Ni- based bimetallic systems with the same ad-metal, in relation to their similar outermost electronic configurations and atomic radius. About ten years ago, another important parameter was pointed out as crucial during the GR process: the size of the M_1 monometallic nanoparticles that should be behind surprising reductions of ions from a M_2 metal less noble than the parent M_1 metal. This behavior opposite to GR was called anti-galvanic replacement (AGR) and was reviewed recently by Astruc's group [60,61]. A description of the reversing of the thermodynamics of the GR reaction as function of the M_1 nanoparticles size was performed by Pattadar *et al*. with the Au-Ag and Au-Pt system where Au, the most noble metal, acts surprisingly here as the reducing M_1 metal [62]. Considering the values of standard reduction potentials, the reactions established in Figure 8 between bulk Au and solution of Ag^+ or $PtCl_4^{2-}$ ions are not thermodynamically favorable under standard conditions, but become dominant with the decrease of the Au nanoparticles from 4.1 to 0.9 nm. Indeed, with the use of anodic stripping voltammetry and STEM-EDS mapping, these authors determined the final composition of the particles obtained after 3 min of AGR with a 10^{-4} mol L^{-1} $AgNO_3$ (or 10^{-5} mol L^{-1} $PtCl_4^{2-}$) solution and obtained the following percentages of Ag (Pt): 17.8 (6.9), 87.2 (35.3) and 100 % for a Au nanoparticles initial diameter of 4.1, 1.6 and 0.9 nm, respectively. For initial diameter of 4.1 and 1.6 nm, bimetallic nanoparticles were obtained with strong metal-metal interactions (Figure 8). Then, from the relative difference in %Ag (Pt) composition obtained as function of size, the authors have concluded that the size-dependent AGR is not simply linked to the number of the available surface atoms, but drived by the decrease in Au oxidation potential with decreasing nanoparticles size, *i.e.* from 0.72 to 0.22 V (*vs* Ag/AgCl, in KBr electrolyte) when the diameter evolves from 4.1 to 0.9 nm. Thus, the AGR strategy has been demonstrated as a novel route for synthesizing alloy nanoclusters difficult to obtain otherwise [63].

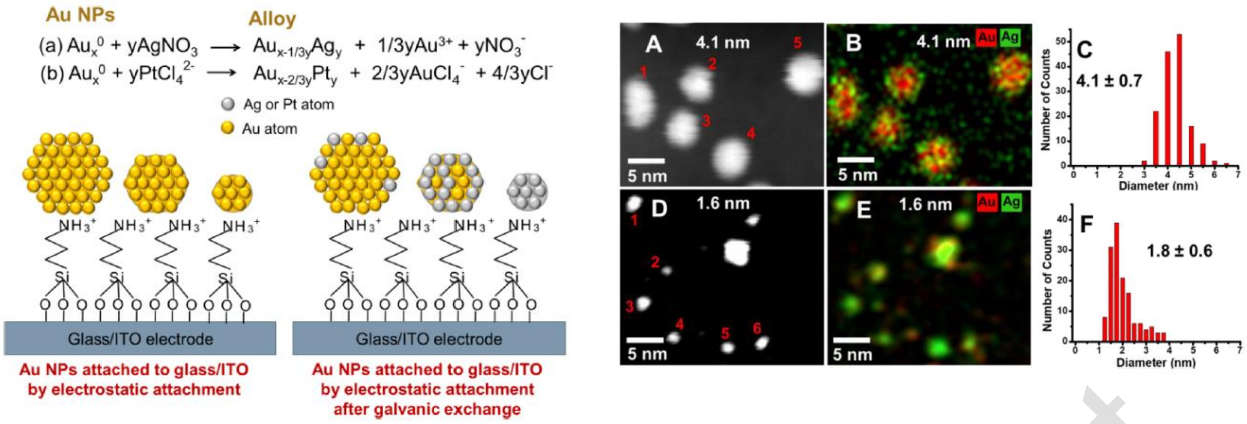

Figure 8. Size-dependent anti-galvanic replacement reaction between Au nanoparticles and Ag ot Pt ions; STEM images (A,D), STEM-EDS mapping images (B,E) and size histograms (C,F) of Au nanoparticles with two different initial sizes (4.1 and 1.6 nm) after AGR with $AgNO_3$ solution. ITO: indium tin oxide. Adapted with permission from Ref. [62]. Copyright © 2020 American Chemical Society.

1.3. Direct redox reaction over supported monometallic nanoparticles

Direct redox reactions are also commonly used to prepare supported bimetallic systems with the aim to improve the catalytic performances compared to the monometallic counterparts by electronic and geometric effects, depending greatly on the shape of the nanoparticles and the atomic arrangement at their surface [64]. Many oxides can be used as support, but one have to keep in mind the possibility for some of them to lead to spontaneous direct redox reaction by simple contact with a metallic precursor salt [36]. It was the case during the preparation of Pt/MnO-Mn_3O_4 catalysts by Kim *et al.* [65], where a Na_2PtCl_4 solution added in suspension with the support was observed to become gradually dark-brown due to the formation of Pt nanocrystals on the surface of the Mn_3O_4 particles. The spontaneous deposition of Pt on Mn_3O_4 was ascribed to the galvanic replacement reaction between $PtCl_4^{2-}$ ions reduced to Pt^0 while part of the Mn_3O_4 was oxidized from oxidation number II to III forming Mn_2O_3 species. Oh *et al.* [66] have also demonstrated that the galvanic replacement process is not exclusively limited to the chemical transformation of metallic nanostructures, since they used this approach to produce hollow box-shaped nanocrystals of Mn_3O_4/γ-Fe_2O_3 *via* oxidation of iron(II) perchlorate by Mn_3O_4. The mechanism implied during the GR reaction between the oxide-based sacrificial template and the modifier metal ions in solution can be sometimes more complex, as put in evidence by Zhu *et al.* [67] for the reductive deposition of Rh (or Pt) on magnetite Fe_3O_4. The authors proposed the mechanism described in Figure 9 where a parallel dissolution and adsorption of Fe^{2+} ions onto the metal occurs leading finally to the formation of FeO_x coated on the Rh nanoparticles supported on Fe_3O_4. The presence of this oxide overlayer allows the metal particle to display efficient redox sites to activate CO_2, favoring its selective reduction to CO.

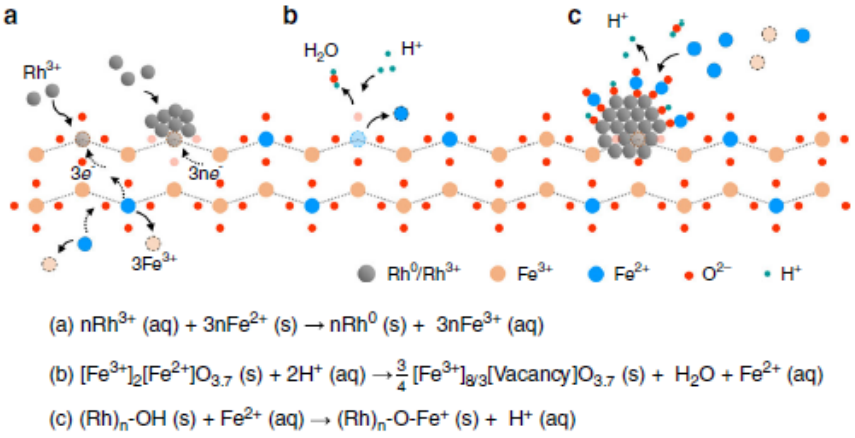

Figure 9. Mechanism during the galvanic replacement reaction between Rh precursor salt and magnetite Fe_3O_4: a) reduction of Rh^{3+} leading to the formation of Rh nanoparticles and oxidation of Fe^{2+} releasing Fe^{3+} ions, b) dissolution of Fe^{2+} species, c) selective deposition of Fe^{2+} ions on Rh nanoparticles. Adapted from Ref. [67].

Classical oxide supports such as Al_2O_3, SiO_2, TiO_2, etc., do not exhibit metallic cations susceptible to be oxidized by contact with a metallic precursor salt belonging to a redox couple of higher potential, leading them totally inert during the preparation of bimetallic catalysts by galvanic replacement method.

On the silica support, Wang et *al.* [68] prepared Ir-Co bimetallic catalysts by direct redox reaction between $IrCl_3$ solution and 10wt.%Co/SiO_2 with the aim to obtain three different Ir contents (0.1, 0.3 and 1.0 wt.%). The surface-decorated systems as-obtained were evaluated for the selective ring opening of methylcyclopentane, revealing a significant higher mass specific rate for the production of 2- and 3-methylpentane and *n*-hexane resulting from the selective cleavage of the endocyclic C-C bonds, compared to monometallic Ir/SiO_2 catalysts of similar Ir contents (Figure 10). By combination of STEM and HRTEM analysis, the distribution of Ir atoms was clearly identified as single atoms or clusters (depending on the Ir content) at the surface of Co nanoparticles with diameters comprised between 2 and 5 nm. Finally, a surface decoration with 0.1wt.% Ir appears as the optimal content in the bimetallic system, highlighting the interest of generating high metal-metal interactions due to highly dispersed catalytically active Ir atoms on the Co surface by GR. Afterward, the same group of researchers followed their investigations on the selective ring opening of methylcyclopentane by preparing trimetallic Pt-Ir-Co/SiO_2 systems *via* galvanic replacement between a solution containing Pt and Ir precursors and Co/SiO_2 catalyst [69].

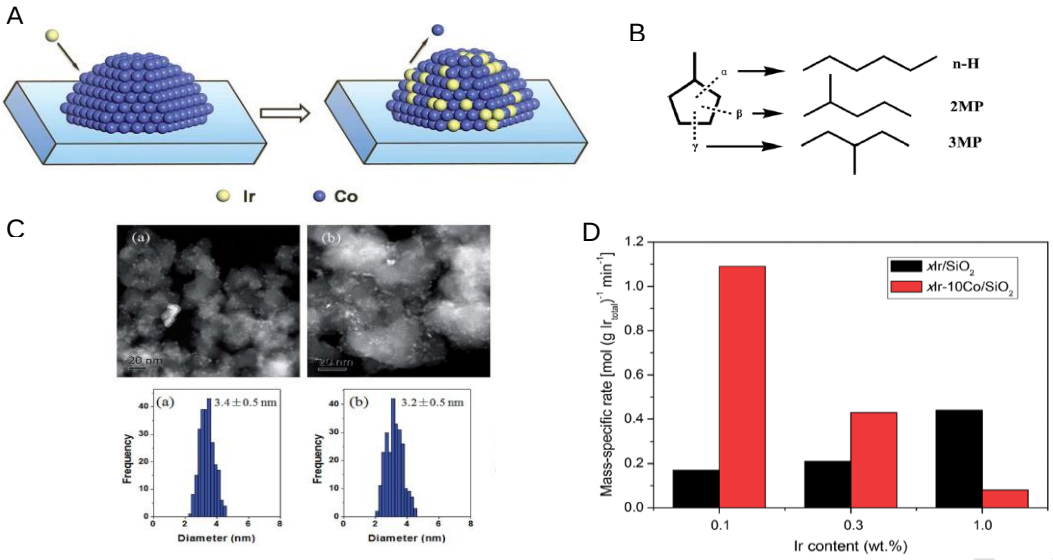

Figure 10. A) Surface-decorated Ir-Co nanoparticles prepared by galvanic replacement from 10wt.%Co/SiO_2 catalyst; B) Selective ring-opening reaction of methylcyclopentane (MCP) towards *n*-hexane (n-H), 2-methylpentane (2MP) and 3-methylpentane (3MP); C) TEM images and particle size distributions for the bimetallic Ir-Co/SiO_2 with (a) 0.3wt.%Ir and (b) 10wt.%Ir; D) Catalytic activity expressed as mass-specific rate corresponding to the molar quantity of MCP converted to nH, 2MP and 3MP per unit of time and Ir content (xIr = nominal weight ratio x of Ir to the catalyst). Adapted with permission from Ref. [68]. Copyright © 2011 Royal Society of Chemistry.

Recently Sun *et al.* [70] have also introduced small quantities of Pd on Ag/Al_2O_3 catalysts by galvanic replacement in order to generate performant systems for the selective hydrodechlorination of 1,2-dichloroethane towards ethylene. For a weight content of the modifier below 0.3wt.%, the Pd atoms remained in an isolated state on the Ag surface as evidenced by CO-IR spectroscopy and XPS analysis, with an electron transfer from Ag to Pd resulting in an intimate bimetallic contact. Such bimetallic structures led to enhanced ethylene selectivity, whereas Pd monometallic displaying large Pd ensembles exhibited a negligible selectivity towards this high valuable product (Figure 11). Aqueous-phase dechlorination of chlorobenzene was also investigated on Ag nanocubes deposited on carbon nanotubes C modified by redox reaction with a $PdCl_2$ solution, leading to high-performant hollow bimetallic nanocubes [71].

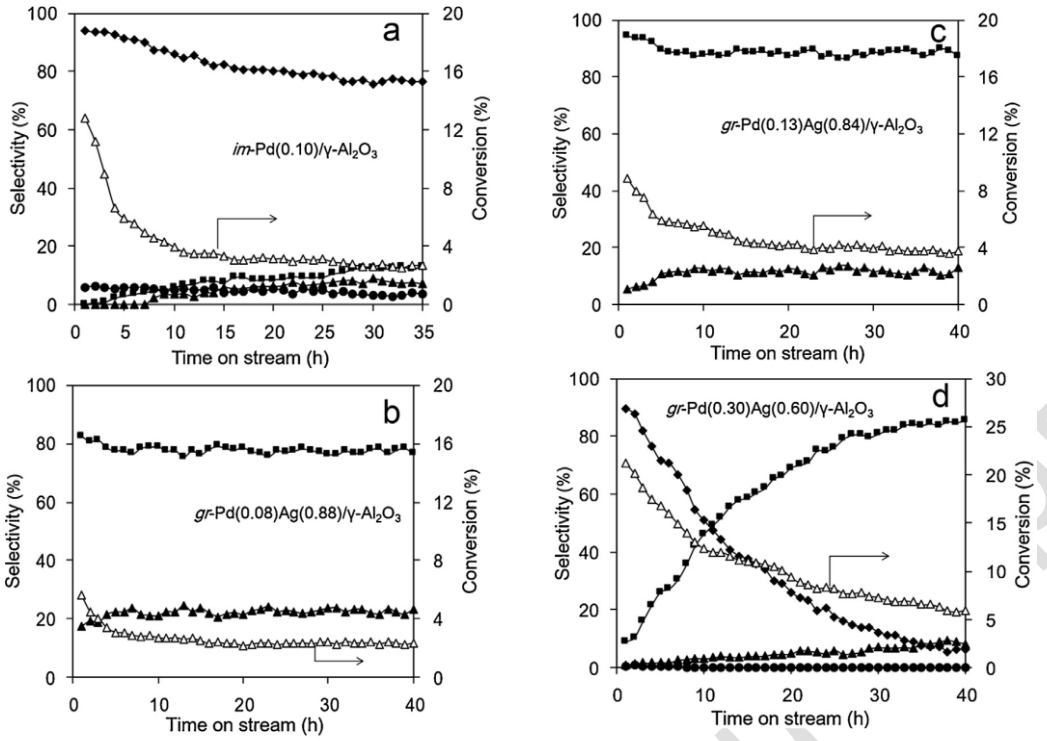

Figure 11. *Catalytic hydrodechlorination of 1,2-dichloroethane as a function of time on stream on: a) monometallic 0.10wt.%Pd/γ-Al₂O₃ prepared by impregnation; b-d) bimetallic Pd-Ag/ γ-Al₂O₃ catalysts prepared by galvanic replacement with three different compositions: (b) 0.08wt%Pd-0.88wt.%Ag, (c) 0.13wt.%Pd-0.84wt.%Ag, (d) 0.30wt.%Pd-0.60wt.%Ag. (■) Ethylene; (♦) Ethane; (▲) Chloroethylene; (●) Chloroethane; (∆) Conversion.* Adapted with permission from Ref. [70]. Copyright © 2018 *E*lsevier.

Once again on alumina support, GR reaction was observed as an excellent method for synthesizing core-shell bimetallic RhNi catalysts active for the CO_2 methanation, compared to the co-reduction (CR) of both Ni and Rh precursor salts introduced simultaneously in solution with polyvinyl alcohol and $NaBH_4$ [72]. XPS, XAS and CO-FTIR characterizations indicated that, with comparable metallic contents (around 1.10wt.%Rh and 1.65wt.%Ni), the GR system displays a thin RhO_x shell encapsulating a Ni core with a strong Rh-Ni synergy, leading to 3.5-fold rate enhancement for CO_2 methanation compared to the CR catalyst constituted of a mix of Rh and RhNi alloy nanoparticles (Figure 12). In other words, Rh highly dispersed over Ni nanoparticles corresponding to a Ni@Rh core-shell structure (GR catalyst) is then superior to Rh alloyed to Ni (CR catalyst) to convert CO_2 selectively to CH_4. Other supported bimetallic catalysts prepared by galvanic replacement process rely on Ni as sacrificial template modified by other metals like Pt to synthesize PtNi/TiO_2 and PtNi /TiO_2-C electrocatalysts for methanol oxidation [73], or Ag to formulate AgNi/C catalysts for the benzylbromide reduction [74] or AgNi/hydrotalcite for methane activation [75]. In this latter case, the direct surface redox reaction was performed between various amounts of $AgNO_3$ precursor and a 12wt.%Ni monometallic catalyst in order to modulate the surface Ag fractions on Ni particles (from 0.03 until 1) leading to well-defined surface Ni-Ag alloys. Replacement of Ni by Ag induced three main effects: (i) it reduces the number of Ni active sites (Ag being inactive for methane activation), (ii) by electronic effect between Ag and Ni, the activity of the remaining accessible Ni sites is also

reduced, (iii) the Ag deposit blocks the active sites responsible for the coke formation (the replacement of only 3 % of the surface Ni atoms by Ag allows decreasing by a factor of ten the carbon yield compared to monometallic Ni).

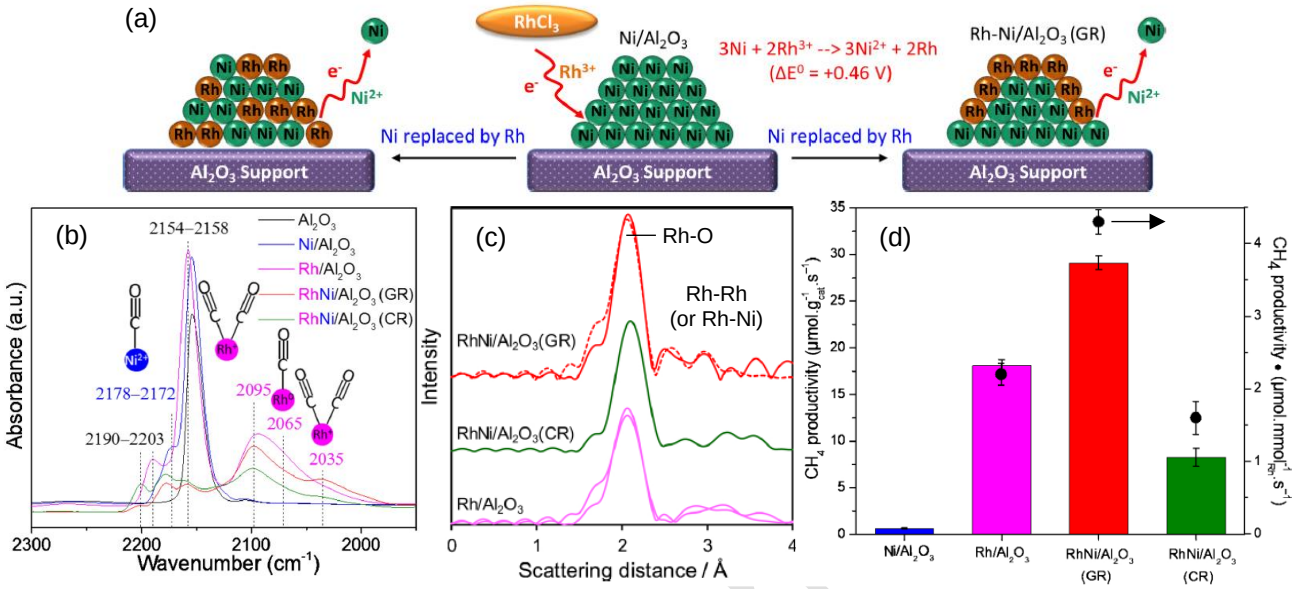

Figure 12. (a) Possible morphologies of the bimetallic $RhNi/Al_2O_3$ catalyst prepared by galvanic replacement (GR) of Ni atoms by Rh; (b) CO-FTIR spectra of monometallic and bimetallic $RhNi/Al_2O_3$ catalysts prepared by GR or co-reduction method (CR); (c) Fourier transform magnitudes of the Rh K-edge EXAFS spectra of monometallic Rh and bimetallic GR and CR $RhNi/Al_2O_3$ catalysts; (d) CH_4 productivity at 250 °C during CO_2 methanation on monometallic and bimetallic $RhNi/Al_2O_3$ catalysts prepared by GR or CR. Adapted with permission from Ref. [72]. Copyright © 2020 Elsevier.

Recently, our group in Poitiers has demonstrated that in the course of the preparation of Co-Re/TiO_2 bimetallic catalysts by successive impregnation of Re precursor salt on Co/TiO_2, a direct redox reaction can occur in agreement with the redox potential values of the involved couples [76]. To demonstrate this galvanic replacement phenomenon, we have prepared two sets of bimetallic samples: the first one by reaction in a beaker between the Re precursor salt (NH_4ReO_4) and a Co/TiO_2 catalyst reduced previously and then exposed to air (usual procedure for the preparation by successive impregnation SI), the second one performed in a appropriated device allowing *in-situ* pre-reduction of the Co/TiO_2 catalyst, letting it under inert atmosphere (N_2) during the contact with the Re solution and filtering of the solution after reaction (conventional protocol used in our lab for the direct surface redox method SR). For a similar Re amount introduced in solution, we obtained a comparable content of Re deposited on both bimetallic samples, but identified clearly a decrease of the Co content on the SR catalysts with the increase of the Re loading. An in-depth characterization of the prepared systems, notably by high-resolution microscopy, temperature-programmed reduction and desorption (TPR and TPD), and CO-FTIR, clearly evidenced the presence of bimetallic Re-Co interactions for both SI and SR samples (Figure 13), but with a contact degree, *i.e.* a metal-metal interaction, and an electron transfer from Re to Co, more pronounced in the case of the

surface redox method. For these catalysts prepared by galvanic replacement where Re species specifically decorate the Co surface, bimetallic particles are obtained with homogeneous size decreasing from 3.3 nm to 1.2 nm when the amount of Re added is increased from 1wt.% to 5wt.% due to the progressive loss of Co atoms, evolving towards a core-shell structure at high Re loading. Conversely, a Janus-type structure predominates on SI catalysts with a concentration of small Re particles around big Co particles.

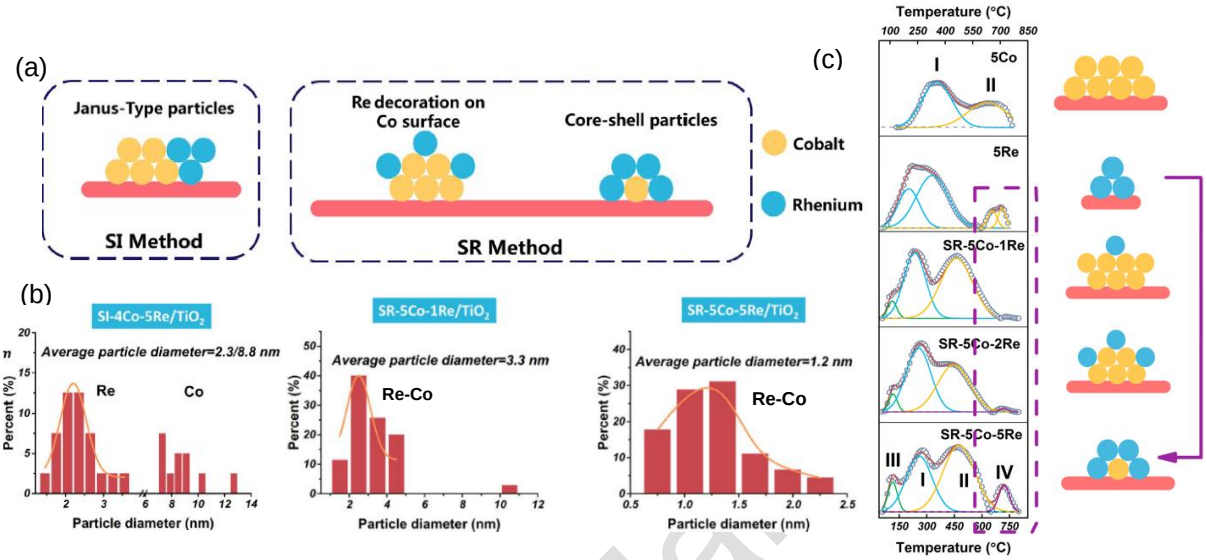

Figure 13. (a) Structures of the bimetallic Co-Re/TiO_2 catalysts prepared by successive impregnation of Re on Co (SI) or direct surface redox reaction (SR); (b) Particle size distribution of SI and SR catalysts deduced from TEM analysis; (c) H_2-TPD profiles of monometallic Co/TiO_2, Re/TiO_2 and bimetallic SR Co-Re/TiO_2 catalysts. Adapted with permission from Ref. [76]. Copyright © 2019 John Wiley and Sons.

The bimetallic interaction was observed to lead to a synergic effect between Co and Re particularly interesting for the selective hydrogenation of citral (α,β-unsaturated aldehyde) to unsaturated alcohols (UA), since the monometallic Co and Re samples, as well as a mechanical mixture of these both catalysts, displayed low activities and UA selectivities compared to bimetallic systems (Table 1).

Table 1. Metal contents of the monometallic Co/TiO_2, Re/TiO_2 and bimetallic Co-Re/TiO_2 catalysts prepared by successive impregnation of Re on Co (SI) or direct surface redox reaction (SR), and catalytic performances for selective hydrogenation of citral to unsaturated alcohols (UA) at 70 °C, under 75 bar, and in isopropanol as solvent.

Catalyst	Co (wt.%)	Re (wt.%)	Activity (mol min^{-1} mol_{met}^{-1})[a]	UA selectivity (%)[b]
5Co	5.3	-	0.1	28
4Co + 1Re[c]	4.0	1.0	0.1	12
SI 4Co-1Re	4.2	1.0	3.6	45
SI 4Co-5Re	4.2	4.5	3.6	45
SR 5Co-1Re	4.0	1.1	0.2	48
SR 5Co-2Re	3.9	1.5	2.6	43
SR 5Co-5Re	2.2	4.8	3.1	52
5Re	-	4.5	1.8	20

(a) Activity = mol of citral transformed/(reaction time*mol of metal)
(b) Selectivity to unsaturated alcohols at 40 % conversion
(c) Physical mixture of 4Co/TiO_2 and 1Re/TiO_2 monometallic catalysts

Other studies in the field of selective hydrogenations have highlighted the interest of galvanic replacement method to achieve efficient bimetallic catalysts, with the aim notably to reduce the precious metal content, these metals being generally the most communly used due to their activity, selectivity and stability in the reaction conditions. One example is the liquid-phase selective hydrogenation of furfural, an important derived lignocellulosic biomass feedstock, for the production of furfuryl alcohol, a value-added chemical (Figure 14a) [77]. Taylor *et al.* used the galvanic replacement to modify the surface of a Cu/γ-Al_2O_3 catalyst by a small quantity of Pt atoms and then prepare a bimetallic Pt_1Cu_{20} system (atomic ratio) exhibiting exceptionally high initial rates of hydrogenation under 10 and 20 bar hydrogen pressure (Figure 14b), rivalling the catalytic performances of monometallic Pt catalyst containing 12 times more Pt, and surpassing the pure Cu and two other bimetallic PtCu catalysts prepared by a colloidal route (with Pt:Cu atomic ratios of 38:62 and 18:82, respectively) (Figure 14c) [77]. For the three studied bimetallic catalysts, a PtCu alloy was evidenced by XRD, TEM and XPS, with an electron transfer from Pt to Cu. However the surface state of the ultra diluted alloy Pt_1Cu_{20} appeared as the most favorable to facilitate hydrogen dissociative adsorption on Pt atoms, and then its spillover onto the Cu atoms where furfural is preferentialy adsorbed.

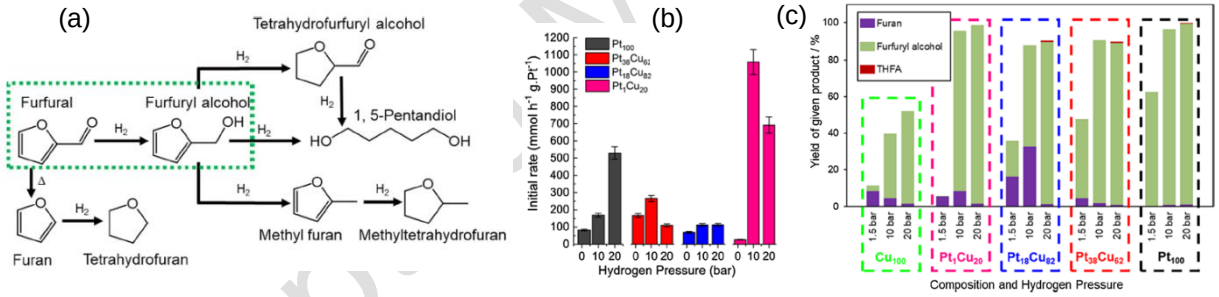

Figure 14. (a) Reactions involved in the transformation of furfural; (b) Normalized initial rates per gram of Pt for monometallic Pt and bimetallic Pt-Cu catalysts supported on alumina; (c) Yield of furan, furfuryl alcohol (targeted product) and tetrahydrofurfuryl alcohol (THFA) obtained after 7 h reaction time with monometallic Pt and Cu catalysts, and bimetallic Pt-Cu catalysts. Pt_1Cu_{20}: bimetallic Pt-Cu/Al_2O_3 catalyst prepared by galvanic replacement; $Pt_{38}Cu_{62}$ and $Pt_{18}Cu_{82}$: bimetallic Pt-Cu/Al_2O_3 catalysts prepared by colloidal route. Reaction conditions: methanol as solvent, 50 °C, three tested hydrogen pressures. Adapted with permission from Ref. [77]. Copyright © 2021 Elsevier.

Another highly efficient bimetallic catalysts for selective hydrogenation reactions were synthesized by galvanic replacement, such as (i) one again for furfural transformation, Pd-Ni/C systems displaying Pd islands on Ni/$Ni(OH)_2$ nanoparticles and showing yield to furfuryl alcohol superior to 90 % at low reaction temperature (5 or 10 °C) with a very good stability, under 5 bar hydrogen pressure and in ethanol solvant, (Figure 15a) [78], (ii) for phenylacetylene hydrogenation, Pd-Co/C systems exhibiting 92 % selectivity to styrene at 93 % conversion, *i.e.* superior performance compared to a Pd-Co alloy catalyst obtained by successive impregnation (Figure 15b) [79], (iii) for benzene conversion to cyclohexene, Ru-M/TiO_2 (M = Fe, Ni, Cu, Co)

nanocomposites obtained by GR followed by acid treatment and leading to Ru species electron-deficient lowering the adsorption strength of cyclohexene on the catalysts and then favoring the selectivity to this product (Figure 15c) [80].

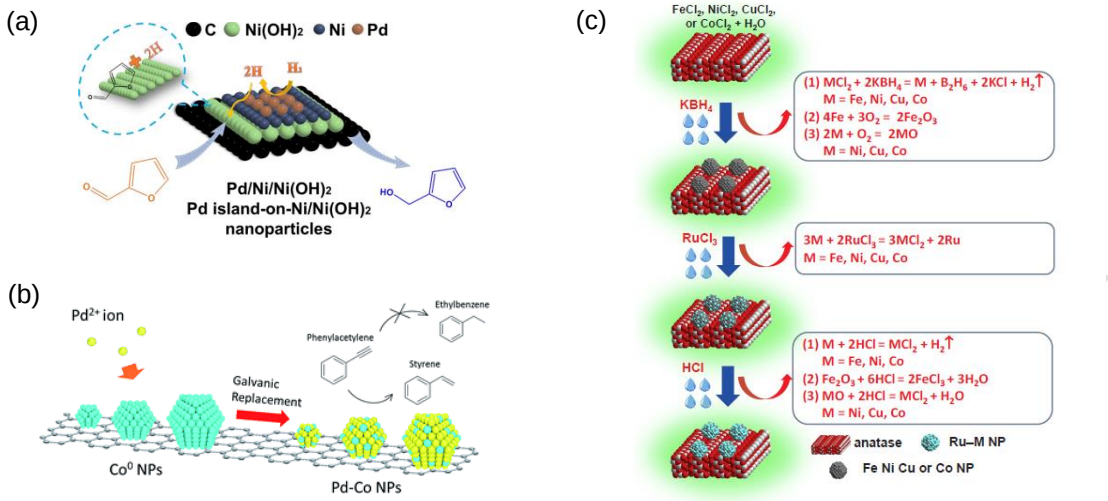

Figure 15. Bimetallic catalysts prepared by galvanic replacement method for selective hydrogenations: (a) Pd-Ni/C catalyst for conversion of furfural to furfuryl alcohol. Adapted with permission from Ref. [78]. Copyright © 2020 Elsevier. (b) Pd-Co/C catalyst for conversion of phenylacetylene to styrene. Adapted from Ref. [79]. (c) Ru-M/TiO_2 catalysts (M = Fe, Ni, Cu, Co) for conversion of benzene to cyclohexene. Adapted with permission from Ref. [80]. Copyright © 2018 Elsevier.

2. Use of an intermediate reducing agent

2.1. Generalities

Another kind of redox reaction used for preparing bimetallic catalysts starting from a monometallic parent supported catalysts consists in using an intermediate reducing agent that is activated at the surface of the monometallic particles (Red*). This process was named "Electroless metal deposition" in 1946 by Brenner and Riddel [81], who described for the first time the proper conditions to deposit a metal onto a metallic surface by catalytic reduction in aqueous solution. This approach is interesting when the direct redox reaction between the base metal M_1 and the promoter M_2 is not thermodynamically possible ($E°(M_2^{m+}/M_2°) < E°(M_1^{n+}/M_1°)$). If the activated reducing agent Red* can be oxidized by M_2^{m+}, *i.e.* if $E°(M_2^{m+}/M_2°) > E°(Ox/Red*)$, the redox process can occur, leading to an oxidized species (Ox), according to the following reaction (4):

$$n\ M_2^{m+} + m\ Red^* \rightarrow n\ M_2° + m\ Ox \quad (4)$$

Contrary to the direct redox reaction, this method may be applied to a large range of metals and does not lead to the dissolution and loss of the parent metal M_1. However, it is of major importance to verify that the metal precursor M_2^{m+} is only reduced at the surface of the parent metal to favour the formation of bimetallic M_1M_2 entities and not on the support or in bulk solution to avoid the formation of monometallic M_2 species.

Many intermediate reducing agents can be used, such as the simplest, hydrogen, and others with lower standard potentials such as formaldehyde, hydrazine, hypophosphite, borohydride or aminoboranes [82].

2.2. Hydrogen as reducing agent

The use of hydrogen for depositing silver, copper and bismuth onto a platinized platinum electrode was firstly reported by Szabo and Nagy in 1976 [83], and named ionization of adsorbed hydrogen. The same principle was then extended to the preparation of supported bimetallic catalysts [84] and developed in Poitiers by Barbier *et al.* [11-17], who have perfected two techniques named refilling (also called recharge) [13,19,20,85-104] and catalytic reduction [95, 105-115]. In the refilling method, the ions of the modifier (M_2^{m+}) are reduced by preadsorbed hydrogen on the parent metal (M_1). The amount of M_2 deposited is then limited by the amount of irreversibly adsorbed hydrogen, *i.e.* limited to a monolayer. Catalytic reduction overcomes this point by continuously introducing hydrogen, enabling larger amounts of M_2 to be deposited, since the hydrogen is activated by M_1, and possibly by M_2 if it is also able to activate H_2, as it is consumed by the redox reaction. Obviously, this method is not possible if M_2^{m+} can be reduced by hydrogen in homogeneous phase. Successive refillings can also be considered to increase the deposition of M_2, when the latter is capable of chemisorbing hydrogen. Thus, many successive refilling steps were used for the first time to deposit the amount of Re needed for usual Pt-Re reforming catalysts [95]. Considering that each rhenium atom deposited poisons a platinum atom, a good correlation was obtained between the experimental rhenium loadings and the theoretical values. Also in Poitiers, we also prepared a series of bimetallic 0.6wt.%Pt–xwt.%Rh/Al_2O_3 by successive refillings of 0.2wt.%Rh onto a monometallic 0.6wt%Pt/Al_2O_3 catalyst and evaluated them for methylcyclopentane ring opening.[116] The addition of successive monolayers of Rh on Pt resulted in nanoparticle growth. We showed that largest particles were more selective for methylcyclopentane ring opening, leading to performance similar to the reference iridium-based catalysts. Recently, we used successive refilling method to deposit Pt on Pt/Al_2O_3 to control the growth of monometallic particles.[117] This method enabled the preparation of uniform Pt particle sizes ranging from 0.95 to 2.62 nm. First, the 1wt.%Pt/Al_2O_3 parent catalyst was prepared by impregnation in basic medium (pH = 11), calcined under air for 4 h at 450 °C and reduced under H_2 at 650 °C during 4 h. For the refilling method, the parent catalyst, previously reduced *in situ* under H_2 during 1 h at 450 °C, was moistened in a volume of water, maintained under H_2 flow to preadsorb hydrogen on the platinum surface (Equation (5)) and then placed under N_2 flow for 15 min to remove dissolved or weakly adsorbed hydrogen in solution and on the catalyst. H_2PtCl_6 solution was then added for a 1 min contact with the parent catalyst, still under N_2 flow (Equation (6)) to perform a redox

reaction between the hydrogen atoms adsorbed at the surface of the Pt parent catalyst and the oxidized Pt species in solution.

$$2\ Pt_s + H_2 \rightarrow 2\ Pt - H \quad (5)$$

$$4\ Pt_s - H + Pt^{4+} \rightarrow Pt\text{-}(Pt_s)_4 + H^+ \quad (6)$$

with Pt_s = surface Pt atoms.

This procedure was repeated up to 3 times to modulate the size of the platinum particles. In fact, by adding the appropriate Pt^{4+}amount, this surface redox reaction induces a uniform growth of the Pt particles (Fig. 16).

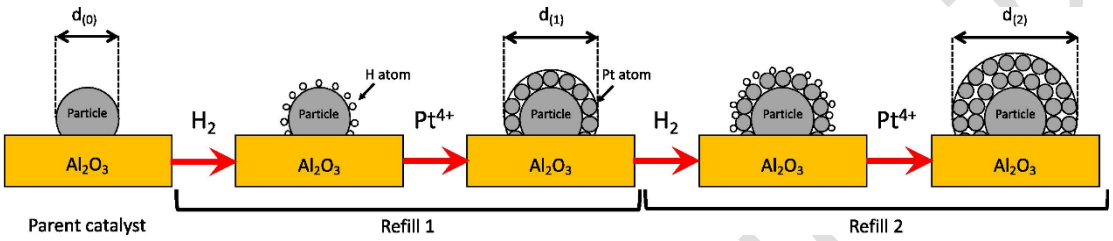

Figure 16. Principle of the refilling method. Reproduced with permission from Ref. [117]. Copyright © 2021 Elsevier.

Controlling the growth of supported Pt nanoparticles from a parent catalyst by the refilling method enabled us to validate a geometric model that quantifies surface site concentrations (corner, edge, face (1 0 0) and face (1 1 1)) for any fcc metal particle size. We demonstrated that the initial activity for propane dehydrogenation reaction was directly correlated with the quantity of corner + edge sites (Fig. 17).

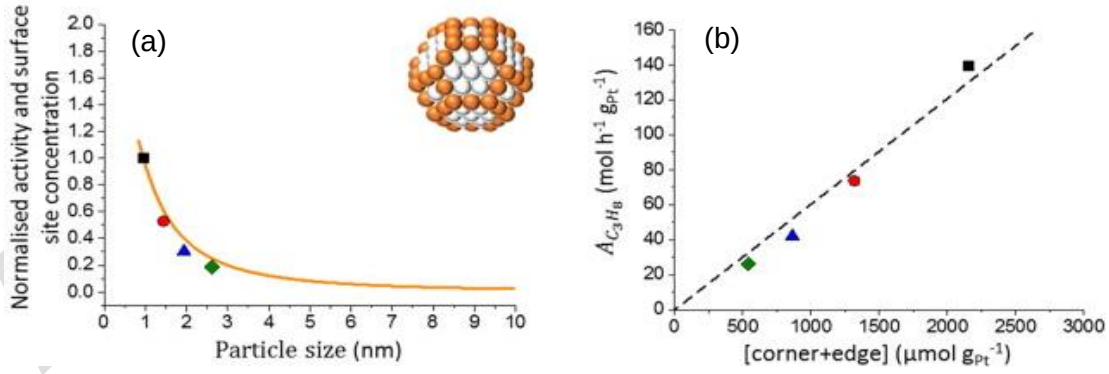

Figure 17. (a) Evolution of the normalized activity for propane dehydrogenation reaction (symbols) and normalized surface site concentrations (corner + edge, orange curve) versus the particle size. (b) Evolution of the initial activity versus corner + edge surface site concentration. Adapted with permission from Ref. [117]. Copyright © 2021 Elsevier.

The catalytic reduction method was investigated for the preparation of different bimetallic catalysts, such as Ru-Cu [105], Ru-Pb [106], Pt-Re [95, 107-110], Pt-Cu [112-115], Pt-Ge [115,118,119], Pt-Sn

[120-122], Pt-Au [123], Pd-Cu [114,124-127], Pd-Ag [114], Pd-Au [114], Pd-Sn [128,129], Pd-In [129], Pd-Re [130-132], Rh-Cu [133], Rh-Ge [118,119].

A study was carried out in our group on Rh-Ge bimetallic systems prepared by catalytic reduction supported on SiO_2, Al_2O_3 and TiO_2.[118,119,134-137]. Unlike their counterparts prepared by successive impregnation, whatever the support, a strong interaction between the metals was confirmed by different techniques like TEM, TPR or by model reaction of cyclohexane dehydrogenation. They were evaluated for the selective hydrogenation of citral, a α,β-unsaturated aldehyde, toward the unsaturated alcohols nerol and geraniol. It was shown that Ge deeply modifies the catalytic properties of Rh and promotes the hydrogenation reaction towards the desired unsaturated alcohols.

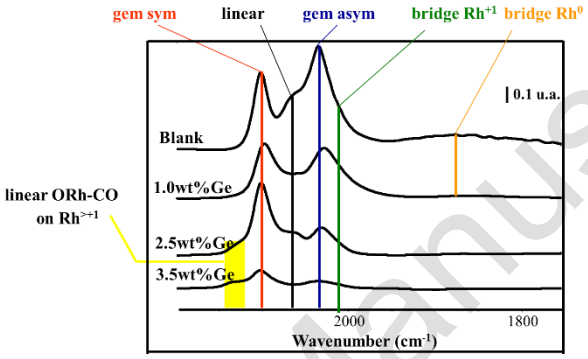

Figure 18. FTIR spectra and peak assignments of adsorbed CO at room temperature on 1wt.%Rh-xwt.%Ge/TiO_2 (x ≥ 0) catalysts reduced at 300 °C. Blank rhodium catalyst was prepared following the same catalytic reduction procedure but without addition of germanium salt.

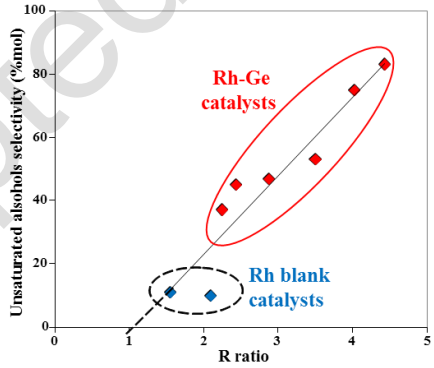

Figure 19. Unsaturated alcohols selectivity as a function of R (R = ΣA(COads on Rh⩾1+ species)/ΣA(COads on total exposed Rh species)) for 1wt.%Rh-xwt.%Ge/TiO_2 (x ≥ 0) catalysts prepared from various metal salt precursors and reduced at 300 °C.

The optimized bimetallic interaction within the Rh-Ge/TiO_2 system was characterized by CO adsorption followed by FTIR. The relative proportion of Rh^0 and $Rh^{\geq 1+}$ species on the surface of the catalysts was determined (Figure 18). To do so a ratio R was calculated; it is defined as the sum of the absolute surfaces of the oxidized rhodium species divided by the sum of the absolute surfaces of the reduced rhodium species. Figure 19 shows the linear evolution of the selectivity in unsaturated alcohols obtained during the hydrogenation of citral as a function of this ratio R for all the samples analysed by FTIR. Thus, the more Rh species oxidized, the

more selective the catalyst in hydrogenating the C=O bond of citral. This evolution evidences that the increase of selectivity in nerol and geraniol, observed after addition of germanium by catalytic reduction, is related to the preferential poisoning of Rh^0 species, which would be the main responsible for the hydrogenation of C=C double bonds. This poisoning is associated with an increase in $Rh^{\geq 1+}$ species, suggesting the existence of a charge transfer from rhodium to germanium favourable to the activation of the carbonyl function of citral. The charge transfer from Rh to Ge was demonstrated by XPS. The catalytic reduction method provided an optimized Rh-Ge bimetallic system for the activation and the selective hydrogenation of the carbonyl function of citral (Figure 20).

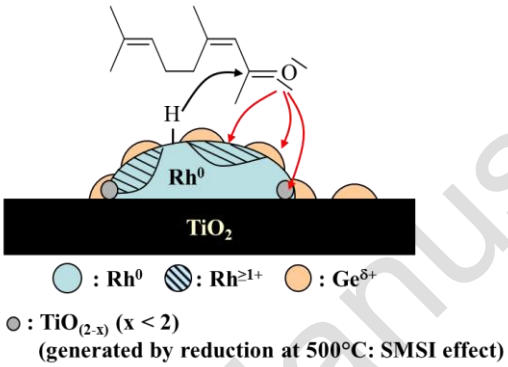

Figure 20. Scheme of a Rh–Ge/TiO_2 catalyst prepared by catalytic reduction highly selective toward the unsaturated alcohols during citral hydrogenation.

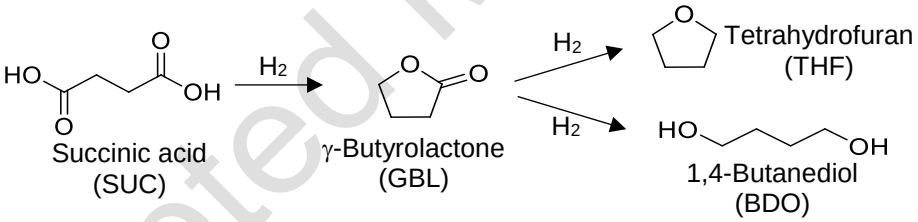

Figure 21. Simplified scheme for the catalytic hydrogenation of succinic acid (SUC) to 1,4-butanediol (BDO).

In the context of biomass valorisation, Pd-Re/TiO_2 catalysts were developed for selective aqueous-phase hydrogenation of succinic acid to 1,4-butanediol (Fig. 21) [130-132]. A 2 wt.%Pd/TiO_2 was modified by addition of various amounts of Re either by successive impregnation or catalytic reduction. The catalytic reduction method led to a selective Re deposition at the Pd–TiO_2 interface while a random one is obtained by successive impregnation (Fig. 22). Moreover, the authors demonstrated that the Re oxidation state depend on the localization of these species: their reduction is complete when they are isolated on the support (Re^0) and maintained partially oxidized (Re^{3+}) when they are in contact with palladium.

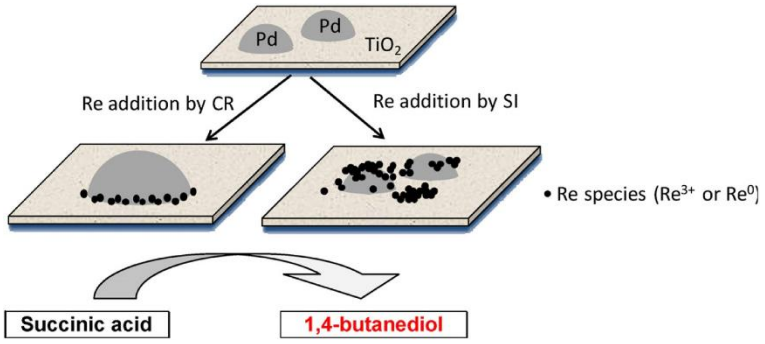

Figure 22. Schematic representation of the Re localization on the Pd/TiO_2 particles according to the preparation method of the bimetallic catalysts: SI, successive impregnation method; CR, catalytic reduction method. Reproduced with permission from Ref. [132]. Copyright © 2020 Elsevier.

It was evidenced that after handling the catalyst in air, Re^{n+} species were partially leached out during heating under Ar in solution in the batch reactor, before introduction of H_2 for the hydrogenation of succinic acid. It appeared that Re^{n+} species re-deposited on the catalyst once under H_2 pressure. The authors took advantage of this fact by developing the preparation of the Pd-Re system by catalytic reduction directly in the batch reactor [131]. For this *in situ* synthesis, monometallic Pd/TiO_2 catalyst was mixed with a NH_4ReO_4 aqueous solution containing different amounts of Re. After purging with Ar, the suspension was heated to 160 °C and the reactor was pressurized under 150 bar H_2 for a given time. A duration of 1 h seemed sufficient and optimal to deposit all the Re species. After cooling and release of the pressure, the aqueous solution of succinic acid was introduced in the batch reactor. After a purge with Ar, the reaction was performed at 160 °C under 150 bar of H_2 pressure. Figure 23 evidences that the catalyst prepared *in situ*, *i.e.* with no contact with air, presents better performances than its counterpart prepared *ex situ*. Therefore, the authors showed that care must be taken to maintain Re-based catalysts under anoxic or reducing conditions to immobilize Re species on their surface and thus maintain their catalytic performance.

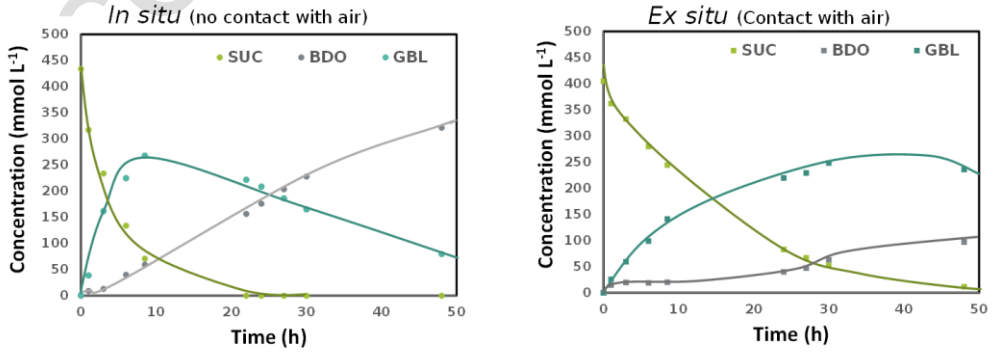

Figure 23. Concentration profiles versus time for succinic acid hydrogenation in the presence of Pd-Re/TiO_2 catalysts prepared by *in situ* and *ex situ* catalytic reduction. SUC: succinic acid, BDO: 1,4-butanediol, GBL: γ-Butyrolactone.

Pd–Sn and Pd–In systems prepared by catalytic reduction were supported on an atypical support: a sulfonated styrene–divinylbenzene copolymer (Sty–DVB), for nitrate removal in

water [129]. TEM of the inner part of the polymer beads shows that metal particles are well distributed with however an apparently higher density of particles in the outer part (Figure 24). The average diameter is about 3 nm, although some aggregates have diameters up to 40 nm. Both bimetallic catalysts were analysed by scanning electron microscopy and the metals were mapped by EDS. The results are shown for Pd–In in Figure 25. The metals are homogeneously distributed on the surface of the copolymer, with no visible agglomeration of palladium, tin or indium metal.

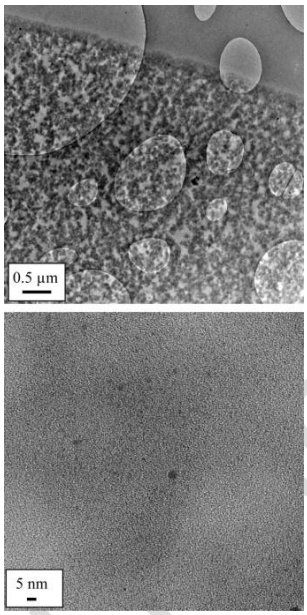

Figure 24. TEM pictures of 5wt.%Pd-5wt.%In/Sty–DVB prepared by catalytic reduction method. Reproduced with permission from Ref. [129]. Copyright © 2013 Elsevier.

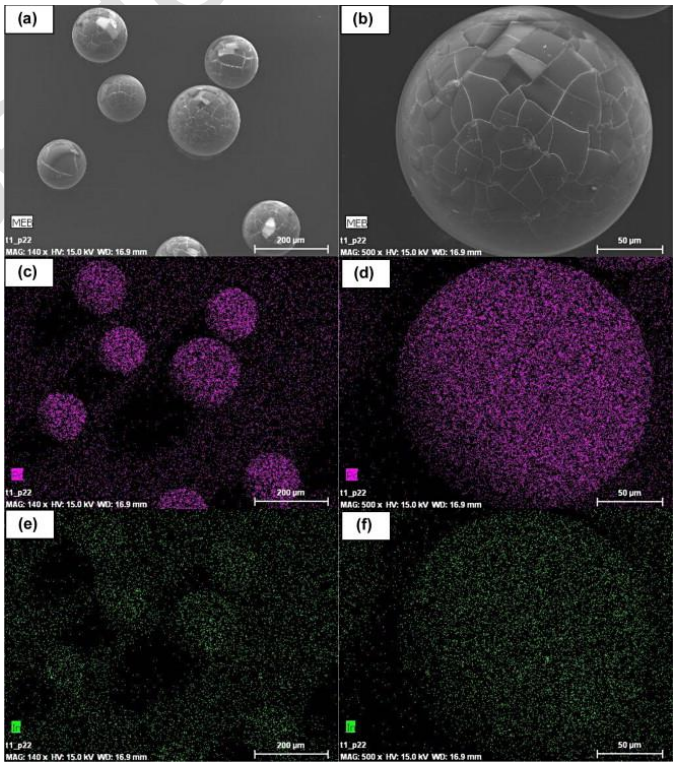

Figure 25. SEM pictures (a and b) and metal mapping (c and d for palladium, e and f for indium) of 5wt.%Pd-5wt.%In/Sty–DVB prepared by catalytic reduction method. Reproduced with permission from Ref. [129]. Copyright © 2013 Elsevier.

Controlling the pH of the solution is the key point in the catalytic reduction of nitrate to avoid the formation of ammonium. In this study, the reaction was performed under pure hydrogen, *i.e.* without any external control of the pH by addition of an acid in the medium. Table 2 compares the performance of Pd–Sn and Pd–In prepared by catalytic reduction to their counterparts, with the same metal loading, prepared by successive impregnation on the copolymer and on an alumina support.

Table 2. Comparison of the catalytic performance at 75 % of nitrate conversion of 5wt.%Pd–2wt.%Sn and 5wt.%Pd–2wt.%In prepared by catalytic reduction (CR) on the copolymer or by successive impregnation (SI) on the copolymer Sty–DVB and on Al_2O_3. Nitrate reduction under pure H_2.

Catalyst	Activity (μmol g^{-1} min^{-1})	Selectivity to N_2 (%)	Final pH
Pd–Sn/Sty–DVB CR	6	72	9.2
Pd–In/Sty–DVB CR	42	12	9.4
Pd–Sn/Sty–DVB SI	5	87	8.9
Pd–In/Sty–DVB SI	14	81	9.3
Pd–Sn/Al_2O_3 SI	32	55	10.0
Pd–In/Al_2O_3 SI	71	52	10.3

Even if the systems prepared by impregnation on Sty–DVB are the most selective to N_2, Pd-Sn catalyst prepared by catalytic reduction is much more selective than catalysts on alumina. We can also notice the lower final pH obtained in the presence of the Sty–DVB support. It was explained that the acid copolymer used as a support could act as a buffer on the catalytic sites where the reaction occurs, thus improving the selectivity towards nitrogen.[129]

The refilling and the catalytic reduction methods also enabled the preparation of trimetallic catalysts, such as Pt-Ir-Sn [121,122], Pt-Ir-Ge [138-140], Pt-Re-Ge [138,140,141], Pt-Re-Sn [142,143], Pd-Sn-Au [144], Pt-Ru-Sn [145], Pt-Ru-Mo [145], Pt-Sn-Te [146], Pt-Sn-Bi [146], Pt-Sn-Au [147], Pt-Sn-Ir and Pt-Sn-Pd [147].

In the area of naphtha reforming, the Szabo's group modified Pt-Sn/γ-Al_2O_3 by addition of Sn, Te, Bi [146] or Au, Ir and Pd [147] by the refilling method whereas Pieck *et al.* , in Santa Fe (Argentina) in collaboration with the group of Poitiers, studied several Pt based trimetallic catalysts prepared by catalytic reduction (Pt-Ir-Ge [138-140], Pt-Re-Ge [138, 140,141], Pt-Re-Sn [142,143]). The results indicate that both methods are suitable for preparing trimetallic catalysts and in general the addition of the third metal modifies the properties of both the metal and acid functions of the bimetallic catalysts. In our laboratory, Pt-Ru-Sn/C and Pt-Ru-Mo/C, prepared by catalytic reduction, were also investigated as anode catalysts with high CO concentration

tolerance for the development of proton exchange membrane fuel cells [145]. The three metals were in strong interaction in the two systems.

2.3. Other reducing agents

Electroless deposition (ED), initially developed in industry for plating metallic surfaces mainly with nickel [148,149], was successfully applied to supported metallic catalysts by the Monnier's group in 2007 for depositing Pt onto Rh/C.[150] Contrary to the method developed by the Barbier's group for which the precursor salt of the second metal is introduced in aqueous solution onto the monometallic catalysts after hydrogen, for ED the reducing agent is dissolved with the precursor salt of M_2 in the electrolytic aqueous solution before introducing the monometallic M_1 parent catalyst. In addition, electroless deposition is often performed at high temperature, generally in the 60-100 °C range, in order to increase the reducing power of the reductant, since the redox potential decreases with temperature. The electrolytic solution may contain in some cases a complexing agent, a stabilizer or a buffer. Complexing agents are generally organic acids or their salt that are chosen as a function of the nature of the second metal M_2 to prevent the precipitation of M_2 in the form of hydroxides and to buffer the solution. For example, acetate, succinate or citrate can be used as complexing agent for electroless deposition of Ni, Co, Pd, Pt or Ru.[148] Stabilizers, such as organic acids, salts of organic acids or heavy metal cations or buffers may also be used to avoid the decomposition of the solution due to an uncontrolled reduction of M_2^{m+} or its precipitation. Various reducing agents can be used for electroless deposition such as aldehydes, carbohydrates, salts of inorganic acids, reducers with weak nitrogen or oxygen single bonds or boron-hydrogen compounds but the most employed are sodium hypophosphite, hydroxylamine, hydrazine, dimethylamine borane, diethylamine borane, sodium borohydride and formaldehyde.[82] It is important to notice that, when the reducing agent contains boron or phosphorus these elements are incorporated in the deposit forming M-B or M-P alloys.[148] One have also to take into account that some of these very efficient reducing agents are very toxic or carcinogenic, as formaldehyde, aminoboranes, hydrazine, sodium borohydrides, and greener reducing agents as those originating from biomass, such as glucose, ascorbic acid or tartrate, should be preferred.

Electroless deposition can be (i) a catalytic process, *i.e.* M_2^{m+} is exclusively reduced at the surface of M_1, or (ii) an autocatalytic process where, once M_2^{m+} is reduced, M_2 in the metallic state may serve as a seed for catalysing the subsequent reduction of M_2^{m+} (Figure 26). Consequently, the catalytic process may favour the formation of core-shell structure while nanoclusters of M_2 may be deposited at the surface of M_1, leaving M_1 atoms accessible, with the autocatalytic process.

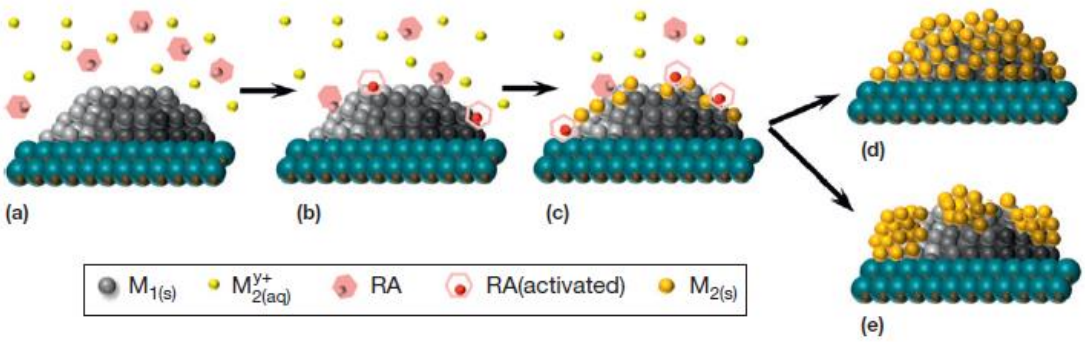

Figure 26. Scheme of electroless deposition method in aqueous solution. (a) Immersion of M_1 monometallic parent catalyst in solution containing the precursor salt of M_2 and the reducing agent RA; (b) Activation of RA at the surface of M_1; (c) Reduction of the precursor salt of M_2; (d) Catalytic reduction at the surface of M_1; (e) Autocatalytic reduction at the surface of M_2. Reproduced with permission from Ref. [151]. Copyright © 2013 Elsevier.

Various mechanisms have been proposed in the literature for electroless plating using various reducing agents in both acid and alkaline media, namely (i) the "atomic hydrogen" mechanism, where the oxidation of the reducing agent leads to chemisorbed hydrogen atoms able to reduce M_2^{m+}, similarly to the reduction process occurring using H_2 as intermediate reducing agent, (ii) the "hydride ion" mechanism, where the reaction of the reducing agent with water or hydroxide ions produces hydride ions that reduce M_2^{m+} leading to M_2^0 and H_2 production, (iii) the "metal hydroxide" mechanism in basic medium involving the reduction of the metal hydroxide by the reduction agent liberating H atoms and (iv) the "electrochemical mechanism" by a direct electron transfer between the reducing agent and M_2^{m+}.[152] In fact all these mechanisms have in common the formation of atomic hydrogen at the surface of the base metal M_1 or the formation of molecular hydrogen during the oxidation of the reducing agent and electroless deposition is favoured on metals M_1 with good hydrogenation/dehydrogenation catalytic properties.[152]

As written above, electroless deposition may be applied to a large range of metals. That means that noble metals may be deposited either by direct redox reaction (galvanic replacement) or by using an intermediate reducing agent (electroless deposition) on a non-noble metal. Consequently, the understanding of reaction mechanism of noble metals deposition onto other transition metals is of major importance to control the growth of the deposit. Pd deposition by redox reaction onto Ni was studied using a Pd^{2+} salt and Ni-P coated Cu (Ni-P/Cu) electrodes in various electrolytic solutions: 1) In the absence of reducing agent; 2) In the presence of a reducing agent, formic acid; 3) In the third experiment the starting electrode was Pd/Ni-P/Cu and Pd^{2+} reduction was performed in the presence of formic acid. The open-circuit potential was measured as a function of time in a three-electrode electrochemical cell in these three experimental conditions (Figure 27).[153]

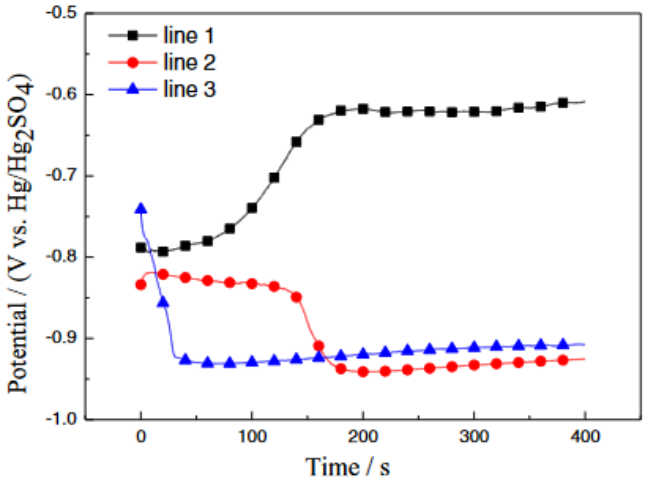

Figure 27. Open circuit potential of Ni-P/Cu electrode in a solution containing $PdSO_4$ and Na_2HPO_4 without reducing agent (line 1 in black) or with formic acid as reducing agent, ethylenediamine and EDTA at 60 °C (line 2 in red) and potential of Pd/Ni-P/Cu electrode in a solution containing $PdSO_4$ and Na_2HPO_4 with formic acid as reducing agent, ethylenediamine and EDTA at 60 °C (line 3 in blue). Reproduced from Ref. [153].

On the Ni-P/Cu electrode, in the absence of formic acid, an increase of potential is observed due to the direct reduction of Pd^{2+} by Ni (galvanic replacement). When the reducing agent is present, the potential decreases slowly during few minutes and then more rapidly to reach a plateau. This particular behaviour was explained by a two-stage reaction process. Initially, only the galvanic replacement is possible at the Ni surface, probably due to the poor ability of Ni to activate formic acid, allowing the deposition of the first Pd atoms that can then activate the reducing agent leading to the complete autocatalytic reaction when the whole surface is covered by Pd atoms, with an intermediate stage where both types of reactions are possible. When the electrode is already covered by Pd (Pd/Ni-P/Cu electrode), the electroless deposition is the only reaction occurring in the presence of formic acid, leading to a sharp decrease in electrode potential.[153]

Electrodeposition can also be used to deposit two metals together at the surface of a substrate. For example, Ni-P-Re alloys were deposited on a copper substrate at T = 70-100 °C from a bath containing $NiSO_4$ and NH_4ReO_4 precursors, hypophosphite as reducing agent and succinate as buffer (pH = 3.0-6.5) and complexing agent.[154] For the same amount of nickel precursor salt introduced in solution, it was shown that the amount of nickel deposited decreased when the amount of rhenium precursor salt was increased. While Ni^0 can only be deposited by reduction of Ni^{2+} by hypophosphite, ReO_4^- can be reduced by both hypophosphite and Ni^0 by galvanic replacement, thus explaining the Re^0 deposition at the expense of that of Ni^0.[154] Furthermore, the simultaneous deposition of two metals is complicated by the fact that the precursors may also interact in solution or at the substrate surface, or be reduced at different reaction rates preventing the deposition of alloys with controlled composition. To overcome this difficulty encountered for Cu-Pt alloys due to the highest reactivity of $PtCl_6^{2-}$, a

strategy was developed based on the engineering of the ligand shell, and the replacement of chloride ions by ethylenediamine thus decreasing the Pt(IV) reactivity. It was demonstrated that this method allowed adjusting the copper to platinum atomic ratio in the alloy by playing with the degree of stabilization of the platinum precursor.[155]

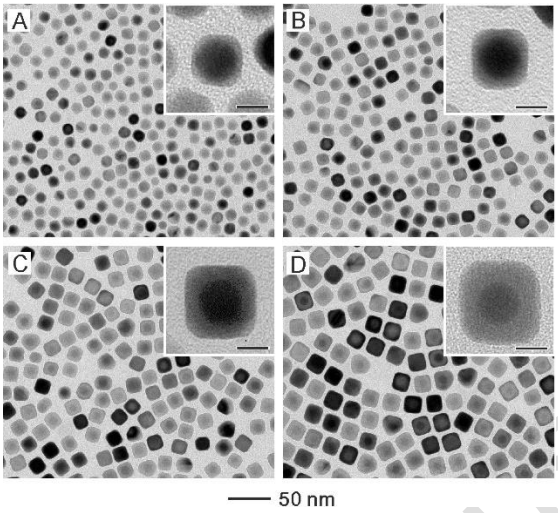

Figure 28. TEM images of Au@Ag core-shell nanocubes obtained by electroless deposition of Au onto Au seeds (spheres of 11 nm diameter, concentration 14.6 mg/L) at 60 °C in aqueous solution containing $AgNO_3$, ascorbic acid as reducing agent and a capping agent, with various volumes of $AgNO_3$ solution (2 mM), added: 0.25 mL (A), 0.5 mL (B), 1 mL (C) and 2 mL (D). Insets are the corresponding high-magnification TEM images with the scale bars being 8 nm. Reproduced with permission from Ref. [156]. Copyright © 2010 American Chemical Society.

It was seen in paragraph 2.2. that Au-Ag nanostructures can be obtained by galvanic replacement by introduction of gold precursors onto Ag nanocubes for example. The inverse is also possible, *i.e.* depositing Ag on Au nanocrystals, not only by anti-galvanic replacement as seen in paragraph 2.2 but also using electroless deposition. In that case, instead of hollow structures as nanoboxes, core-shell structures are obtained. Thus, starting from Au seeds, Au@Ag core-shell nanocubes were obtained in aqueous solution containing $AgNO_3$ as Ag precursor salt, ascorbic acid as reducing agent and cetyltrimethylammonium chloride as capping agent. The thickness of Ag shells was varied by controlling the ratio $AgNO_3$/Au seed in the aqueous solution (Fig. 28).[156]

While the literature on electroless plating for depositing thin layers of metals on a substrate is abundant, the one on surface modification of supported metal nanoparticles for the preparation of bimetallic catalysts is much more limited, and mainly carried by Monnier's group at the University of South Carolina (USA) for preparing Pt-Rh/C [150], Cu-Pd/SiO_2 [157,158], Au-Pd/SiO_2 [159], Au-Pd/C [160], Ag-Pd/SiO_2 [159], Ag-Pt/SiO_2 [161], Pt-Pd/C [162], Pt-Co/C [159], Au-Pd/SiO_2 [163], Pt-Ru/C [164], Ni-Pt/Al_2O_3 [165] etc. and even trimetallic catalysts such as Pd@Cu-Pt/C with a Cu-Pt mixed-metal shell [166]. These systems were successfully applied as electrocatalysts for fuel

cell applications [150,166] or as catalysts for methane dry reforming (Ni-Pt/Al_2O_3) [165] or glycerol oxidation in liquid phase (Au-Pd/C) [160].

When electroless deposition is performed to modify supported monometallic catalyst, one have to keep in mind that the precursor salt of second metal M_2^{m+} may also be deposited on the support by electrostatic adsorption. To avoid this phenomenon, the pH of the deposition solution must be chosen as a function of the point of zero charge of the support and of the ionic form (cation or anion) of the precursor salt. The pH has also a strong impact on the choice of the reducing agent: for example, sodium borohydride is basic and decomposes in acidic medium, and can only be used in basic medium. Consequently, acidic reducing agent must be chosen for electroless deposition at low pH. Thus, deposition of $Ru(NH_3)_6^{3+}$ onto 20wt.%Pt/C was performed at pH lower than the pzc of the carbon support (pH = 4.8) in the presence of formic acid, ensuring that the surface of the support is positively charged, avoiding any interaction with the Ru precursor salt.[164] It must also be verified that the reduction of the precursor takes place on the surface of the M_1 metal and not in solution. It was demonstrated that at low pH the amount of Ru species remains stable in solution in the presence of formic acid (FA) until the introduction of the monometallic Pt/C catalyst marking the beginning of electroless deposition (Figure 29). Finally, deposition rate is strongly dependent on the reaction temperature and at 120 °C the deposit of Ru is complete in less than 5 min (30 min at 110 °C) (Figure 29).

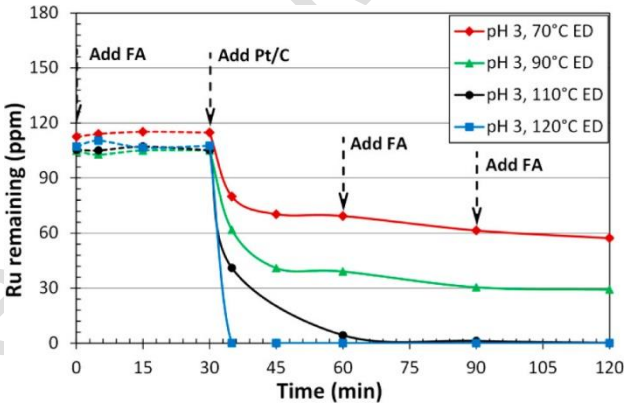

Figure 29. Ru remaining as a function of time in aqueous solution of $Ru(NH_3)_6Cl_3$ in the presence of formic acid (FA) and monometallic Pt/C catalyst (added at t 30 min) at pH 3 and various temperatures. Reproduced with permission from Ref. [164]. Copyright © 2015 American Chemical Society.

However, depending on the reactivity of the metal precursor and the reducing agent, it is in some cases very difficult to avoid the reduction of M_2^{m+} in solution and the addition of a chelating and stabilizing agents is not always sufficient, especially for noble metals of which metal precursor are very rapidly reduced in aqueous solution. To avoid this phenomenon, a synthesis strategy has been developed for obtaining core-shell catalysts by depositing approximately 1 to 3 monolayers (ML) of Pt at the surface of Pd nanoparticles on a carbon support (30wt.%Pd/C).[167] This necessitates huge amount of Pt precursor salt (H_2PtCl_6) in

solution and consequently to choose very high concentrations of reducing agent. Hydrazine was chosen for its low redox potential, -0.92 V/SHE at 25 °C and pH 9, and because its oxidation only yields gaseous products, N_2 and H_2, avoiding any pollution by organic residues. Instead of introducing all the components, *i.e.* the precursor salt, the complexing agent, the ethylenediamine, the reductant and the monometallic catalyst in the same electrolytic bath, the hydrazine was added progressively by means of a pump. This process, named semi-continuous electroless deposition, allowed obtaining core-shell Pt-Pd/C catalyst (Fig. 30) from 0.9 to 3.4 ML of Pt which demonstrated better activity for oxygen reduction reaction than Pt/C.

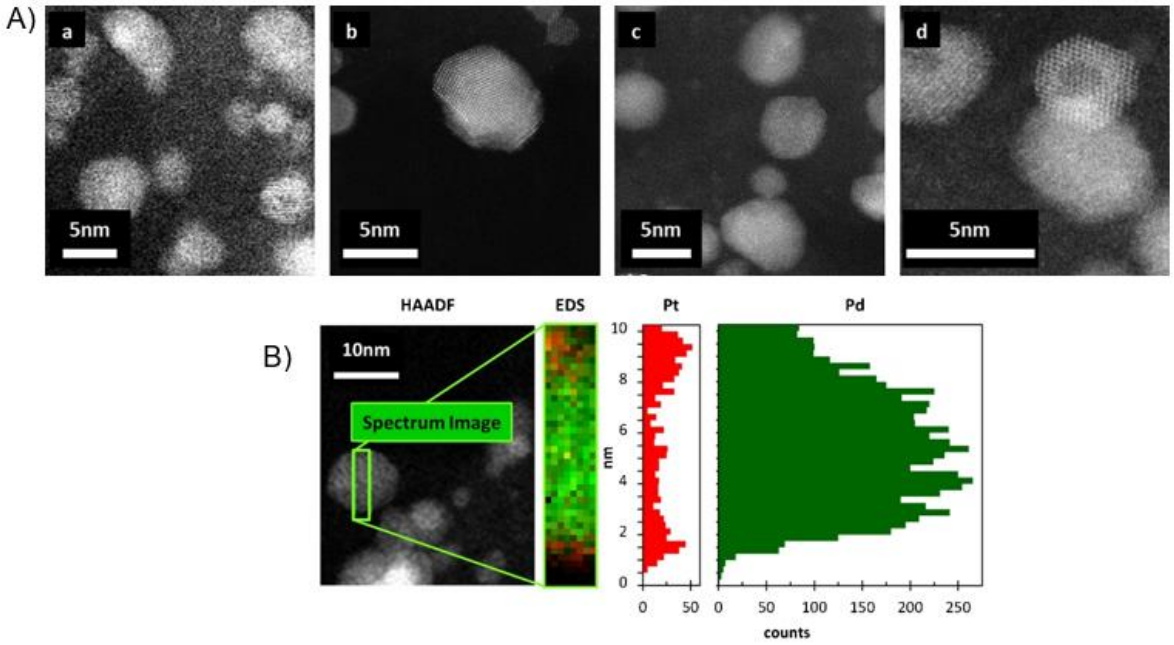

Figure 30. A) HAADF images of core-shell Pt-Pd/C bimetallic catalysts with various ML of Pt over 30wt.%Pd/C: (a) ML = 0; (b) ML = 0.9; (c) ML = 1.7; (d) ML = 2.7. B) HAADF of 2.7 ML Pt on Pd/C, EDS sectional elemental analysis, EDS line scan of Pt (red) and of Pd (green). Reproduced with permission from Ref. [167]. Copyright © 2016 Elsevier.

3. Concluding remarks and outlook

The preparation of bimetallic supported catalysts by redox reactions ensures the selective deposition of the second metal M_2 at the surface of monometallic M_1 nanoparticles favoring high metal-metal interactions.

Direct redox reaction, or galvanic replacement, is an interesting way to deposit noble metals such as Pt at the surface of other transition metals, such as Cu, Ni or Co, easy to perform and which can be used to decrease the size of the bimetallic nanoparticles compared to the parent monometallic catalyst due to the inevitable loss of the base metal. However, this method depends on the redox potential of the two metals involved in the reaction and can only be applied for a limited number of M_1-M_2 pairs. The use of an intermediate reducing agent opens up more possibilities, even if, compared to galvanic replacement, more parameters should be

carefully adjusted to control the deposition, such as the particle size of M_1 and consequently its capacity of adsorbing intermediate reducing agent. This method, generally called electroless deposition or, in the case of the H_2, catalytic reduction or refilling method, allows the preparation of a wide range of bimetallic catalysts. Indeed, in this case the redox reaction is governed by the choice of the reducing agents and other components such as complexing agents, stabilizers, buffers etc. and by the ability of the base metal M_1 to activate it. Thus, non-noble metals can be deposited on the surface of noble metals and there is no loss of the base metal M_1 since it is not involved in the redox reaction. These bimetallic catalysts have demonstrated high catalytic activities in a wide range of reactions due to the high metal-metal interactions generated by the redox process.

The last few years have seen the emergence of new types of catalysts, based on the presence of isolated atoms at the surface of a support, namely single-atom catalysts (SACs) [168-172], or at the surface of metallic nanoparticles, namely single-atom alloys (SAAs) [173-175]. In general SACs and SAAs are obtained by using trace amounts of an active metal of which atoms are stabilized by the support or the host metal. They have demonstrated higher activities than their counterpart in the form of nanoparticles for many reactions and constitute a promising way for decreasing the use of critical materials such as noble metals. While SACs suffer a lack of stability, at high temperature especially under reducing atmosphere, the strong metal-metal interaction in SAAs allows conferring to these systems a better thermal stability maintaining single-atoms isolated. Given the ultralow amount of the second metal M_2 added to the host metal M_1, it is of major importance that the active metal M_2 is dispersed on the surface of M_1 ensuring 100 % accessibility to the reagents. For this reason, redox methods, and more specifically galvanic replacement which allows the replacement of M_1 surface atoms with M_2 atoms, are the methods of choice especially when M_2 is a more noble metal than M_1. Thus, the first SAAs reported in the literature, $Pd0.18Cu15/Al_2O_3$, were synthesized by direct reduction of H_2PtCl_6 on the surface of copper nanoparticles [176]. In addition to SAAs, redox methods allow the preparation of bimetallic catalysts with reduced critical metal contents by offering the possibility to deposit them selectively on the surface of other metals and optimizing their accessibility and stability. Consequently, these methods should meet with renewed interest in the future.

List of abbreviations:

- AGR: Anti-Galvanic Replacement
- DR: Direct Redox reaction
- ED: Electroless Deposition
- EDS: Energy Dispersive X-ray Spectroscopy
- EDTA: EthyleneDiamineTetraacetic Acid
- EXAFS: Extended X-Ray Absorption Fine Structure
- FTIR: Fourier Transformed Infra-Red
- GR: Galvanic Replacement

- HAADF: High-Angle Annular Dark Field
- HR-TEM: High Resolution Transmission Electron Microscopy
- ML: Monolayer
- NP: NanoParticle
- ORR: Oxygen Reduction Reaction
- PEMFCs: Proton Exchange Membrane Fuel Cells
- PVP: PolyVinylPyrrolidone
- RA: Reducing Agent
- SAAs: Single-Atom Alloys
- SACs: Single-Atom Catalysts
- SEM: Scanning Electron Microscopy
- SHE: Standard Hydrogen Electrode
- SI: Successive Impregnation
- SR: Surface Redox reaction
- STEM: Scanning Transmission Electron Microscopy
- Sty–DVB: Styrene–DiVinylBenzene
- SUC: Succinic Acid
- TEM: Transmission Electron Microscopy
- THFA: TetraHydroFurfuryl Alcohol
- TPD: Temperature Programmed Desorption
- TPR: Temperature Programmed Reduction
- UA: Unsaturated Alcohol
- XAS: X-ray Absorption Spectroscopy
- XPS: X-ray Photoelectron Spectroscopy
- XRD: X-Ray Diffraction

References

[1] G.M. Schwab, *Discuss. Faraday Soc.*, **1950**, *8*, 166-171.
[2] A. Couper, D.D. Eley, *Discuss. Faraday Soc.*, **1950**, *8*, 172-184.
[3] D.A. Dowden, P.W. Reynolds, *Discuss. Faraday Soc.*, **1950**, *8*, 184-190.
[4] D.A. Dowden, *J. Chem. Soc.*, **1950**, 242-265.
[5] W.M.H. Sachtler, P. Van der Plank, *Surf. Sci.*, **1969**, *18*, 62-79.
[6] H.E. Kluksdahl, U.S. Patent 3,415,737, **1968**.
[7] G. Leclercq, D. Jaunay, R. Maurel, *J. Chem. Res.*, **1979**, *2*, 62-63.
[8] V. Ponec, G.C. Bond, *Studies in Surface Science and Catalysis*, **1995**, *95*, 477-539.
[9] O.P. Tkachenko, L.M. Kustov, S.A. Nikolaev, V.V. Smirnov, K.V. Klementiev, A.V. Naumkin, I.O. Volkov, A.Y. Vasil'kov, D.Y. Murzin, *Top. Catal.,* **2009**, *52*, 344-350.
[10] A.G.M. da Silva, T.S. Rodrigues, S.J. Haigh, P.H.C. Camargo, *Chem. Commun.*, **2017**, *53*, 7135-7148.
[11] C. Montassier, J.C. Menezo, J. Moukolo, J. Naja, L.C. Hoang, J. Barbier, J.P. Boitiaux, *J. Mol. Catal.*, **1991**, *70*, 65-84.
[12] J. Barbier, Catalytica Studies Division, *Advances in Catalysts Preparation*, Study Number 4191 CP, **1992**.
[13] J. Barbier, P. Marécot, G. Del Angel, P. Bosch, J.P. Boitiaux, B. Didillon, J.M. Dominguez, I. Schiftef, G. Espmosa, *Appl. Catal. A: Gen.*, **1994**, *116*, 179-186.
[14] J. Barbier, in *Handbook of Heterogeneous Catalysis*, Vol.1 (Eds G. Ertl, H. Knözinger, J. Wertkamp) Wiley-VCH, Weinheim, pp 257-264, **1997**.
[15] J. Barbier, M.J. Chollier, F. Epron, in *Catalysis by metals* (Ed. A.J. Renouprez and H. Jobic) Les Editions de Physique, Springer-Verlag, pp 113-131, **1997**.
[16] C.L. Pieck, P. Marécot, J. Barbier, *Appl. Catal. A: Gen.*, **1996**, *134*, 319-329.
[17] F. Epron, C. Especel, G. Lafaye, P. Marécot, in *Nanoparticles and Catalysis* (Ed. Didier Astruc), Wiley-VCH, pp 279-302, **2008.**
[18] X. Xia, Y. Wang, A. Ruditskiy, Y. Xia, *Adv. Mater.,* **2013,** *25*, 6313-6333.
[19] C. Micheaud, M. Guerin, P. Marecot, C. Geron, J. Barbier, *J. Chim. Phys.*, **1996**, *93*, 1394-1411.

[20] C. Micheaud, P. Marécot, M. Guérin, J. Barbier, *Appl. Catal. A: Gen.*, **1998**, *171*, 229-239.
[21] M.C. Daniel, D. Astruc, *Chem. Rev.,* **2004**, *104*, 293-346.
[22] C.J. Murphy, T.K. Sau, A.M. Gole, C.J. Orendorff, J. Gao, L. Gou, S.E. Hunyadi, T. Li, *J. Phys. Chem. B*, **2005**, *109*, 13857-13870.
[23] J. Park, J. Joo, S.G. Kwon, Y. Jang, T. Hyeon, *Angew. Chem., Int. Ed*., **2007**, *46*, 4630-4660.
[24] Y. Xia, Y. Xiong, B. Lim, S.E. Skrabalak, *Angew. Chem. Int. Ed*., **2009**, *48*, 60-103.
[25] A. Dursun, D. Pugh, S. Corcoran, *J. Electrochem. Soc.*, **2003**, 150, B355-B360.
[26] J. Greeley, J. Norskov, *Electrochim. Acta*, **2007**, 52, 5829-5836.
[27] M.A. Mahmoud, D. O'Neil, M.A. El-Sayed, *Chem. Mater.*, **2014**, *26*, 44-58.
[28] A. Ruditskiy, H.C. Peng, Y. Xia, *Annu. Rev. Chem. Biomol. Eng.*, **2016**, *7*, 327-348.
[29] M.H. Sun, S.Z. Huang, L.H. Chen, Y. Li, X.Y. Yang, Z.Y. Yuan, B.L. Su, *Chem. Soc. Rev.*, **2016**, *45*, 3479-3563.
[30] G. Prieto, H. Tüysüz, N. Duyckaerts, J. Knossalla, G.H. Wang, F. Schüth, *Chem. Rev.,* **2016**, 116, 14056-14119.
[31] F. Yan, Z. Hu, Q. Tian, B. Wang, *Inorg. Chem. Commun.*, **2020**, *116*, 107896.
[32] X. Zhang, C. Lian, Z. Chen, Y. Li, *Nano Res.,* **2018**, *11*, 4142-4148.
[33] B. Goris, L. Polavarapu, S. Bals, G. Van Tendeloo, L.M. Liz-Marzán, *Nano Lett.,* **2014**, *14*, 3220-3226.
[34] J.G. Smith, I. Chakraborty, P.K. Jain, *Angew. Chem. Int. Ed.,* **2016**, *55*, 9979-9983.
[35] S.W. Chee, S.F. Tan, Z. Baraissov, M. Bosman, U. Mirsaidov, *Nat. Commun*., **2017**, *8*, 1224.
[36] B. Zhao, X. Guo, W. Zhao, J. Deng, B. Fan, G. Shao, Z. Bai, R. Zhang, *Nano Res.,* **2017,** *10***,** 331-343.
[37] W. Wang, M. Dahl, Y. Yin, *Chem. Mater.*, **2013**, *25*, 1179-1189.
[38] X. Wang, J. Feng, Y. Bai, Q. Zhang, Y. Yin, *Chem. Rev.*, **2016**, *116*, 10983-11060.
[39] J. Zeng, Q. Zhang, J. Chen, Y. Xia, *Nano Lett.*, **2010**, *10*, 30-35.
[40] T.J.A. Slater, A. Macedo, S.L.M. Schroeder, M.G. Burke, P. O'Brien, P.H.C. Camargo, S.J. Haigh, *Nano Lett.*, **2014**, *14*, 1921-1926.
[41] S. Wang, J. Yin, H. Wei, K. Huang, L-M. Liu, H. Wu, *ACS Appl. Energy Mater.,* **2019**, *2*, 468-476.
[42] N. Naresh, P. Karthik, R. Vinoth, C. Muthamizhchelvan, B. Neppolian, *Electrochim. Acta*, **2018**, 282, 792-798.
[43] L.E. Mathurin, M. Benamara, J. Tao, Y. Zhu, J. Chen, *Part. Part. Syst. Charact.*, **2018,** *35(5),* 1800053.
[44] X. Wang, S. Chen, G. Reggiano, S. Thota, Y. Wang, P. Kerns, S.L. Suib, J. Zhao, *Chem. Commun.,* **2019**, *55*, 1249-1252.
[45] Y. Wang, C. Wang, H. Shang, M. Yuan, Z. Wub, J. Li, Y. Du, *J. Colloid Interface Sc.,* **2022**, *605*, 779-789.
[46] K.D. Gilroy, A. Ruditskiy, H.C. Peng, D. Qin, Y. Xia, *Chem. Rev.*, **2016**, *116*, 10414-10472.
[47] Y. Yang, Q. Zhang, Z. Fu, D. Qin, *ACS Appl. Mater. Interfaces*, **2014**, *6*, 3750-3757.
[48] F. Merkoçi, J. Patarroyo, L. Russo, J. Piella, A. Genç, J. Arbiol, N.G. Bastús, V. Puntes, *Mater. Today Adv.,* **2020,** *5,* 100037.
[49] L. Wang, Z. Zeng, C. Ma, Y. Liu, M. Giroux, M. Chi, J. Jin, J. Greeley, C. Wang, *Nano Lett.,* **2017,** *17,* 3391-3395.
[50] J.Y. Jung, D.G. Kim, I. Jang, N.D. Kim, S.J. Yoo, P. Kim, *J. Indus. Eng. Chem.,* **2022,** *111,* 300-307.
[51] M.C. França, R.M. Ferreira, F. dos Santos Pereira, F. Anchieta e Silva, A.C. Azevedo Silva, L.C. Silva Cunha, J. de Jesus Gomes Varela Júnior, P. de Lima Neto, A. Atsushi Takana, T. Silva Rodrigues, M.A. Suller Garcia, *J. Mater. Sci.,* **2022,** *57***,** 8225-8240.
[52] S. Papadimitriou, S. Armyanov, E. Valova, A. Hubin, O. Steenhaut, E. Pavlidou, G. Kokkinidis, S. Sotiropoulos, *J. Phys. Chem. C,* **2010,** *114,* 5217-5223
[53] H. You, L. Zhao, Y. Zuo, J. Fang, *Part. Part. Syst. Char.,* **2022,** *39 (2),* 2100248.
[54] H. Lei, X. Li, C. Sun, J. Zeng, S. Singh Siwal, Q. Zhang, *Small,* **2019**, *15*, 1804722.
[55] Y. Kobayashi, Z. Cai, G. Chang, Y. He, M. Oyama, *ACS Appl. Energy Mater.,* **2019**, 2, 6023-6030.
[56] D. Li, Z. Zong, Z. Tang, Z. Liu, S. Chen, Y. Tian, X. Wang, *ACS Sustainable Chem. Eng.*, **2018**, 6, 5105-5114.
[57] A. Kumar, S. Deka, *Appl. Catal. A: Gen.,* **2020**, *599*, 117575.
[58] B.T. Jebaslinhepzybai, N. Prabu, M. Sasidharan, *International J. Hydrogen Energy,* **2020**, *45*, 11127-11137.
[59] S. Wang, J. He, J. Xie, Y. Zhu, Y. Xie, J.G. Chen, *Appl. Surf. Sci.,* **2008**, *254*, 2102-2109.
[60] X. Liu, D. Astruc, *Adv. Mater*., **2017**, *29*, 1605305.
[61] X. Liu, J. Ruiz, D. Astruc, *Chem. Commun.,* **2017**, *53*, 11134.
[62] D.K. Pattadar, R.A. Masitas, C.D. Stachurski, D.E. Cliffel, F.P. Zamborini, *J. Am. Chem. Soc.,* **2020**, *142*, 19268-19277.

[63] M. Zhu, P. Wang, N. Yan, X. Chai, L. He, Y. Zhao, N. Xia, C. Yao, J. Li, H. Deng, Y. Zhu, Y. Pei, Z. Wu, *Angew. Chem. Int. Ed.,* **2018**, *57,* 4500-4504.
[64] D. Kim, J. Resasco, Y. Yu, A.M. Asiri, P. Yang, *Nat. Commun.,* **2014**, *5*, 4948.
[65] K.W. Kim, S.M. Kim, S. Choi, J. Kim, I.S. Lee, *ACS Nano,* **2012**, 6 (6), 5122-5129.
[66] M.H. Oh, T. Yu, S.H. Yu, B. Lim, K.T. Ko, M.G. Willinger, D.H. Seo, B.H. Kim, M.G. Cho, J. H. Park, K. Kang, Y.E. Sung, N. Pinna, T. Hyeon, *Science*, **2013**, *340*, 964-968.
[67] Y. Zhu, X. Zhang, K. Koh, L. Kovarik, J.L. Fulton, K.M. Rosso, O.Y. Gutiérrez, *Nat Commun.,* **2020,** *11,* 3269.
[68] Z. Wang, A. Zheng, R. Zheng, M. Li, H. Li, G. Xu, G. Xia, *RSC Adv.,* **2016,** *6,* 105063-105069.
[69] X. Dong, P. Zheng, A. Zheng, H. Li, G Xia, M. Li, R. Zheng, B. Xu, *Catal. Today,* **2018,** *316,* 162-170.
[70] J. Sun, Y. Han, H. Fu, H. Wan, Z. Xu, S. Zheng, *Appl. Surf. Sc.,* **2018,** *428,* 703-709.
[71] G. Hu, S. Lai, C. Ye, A. Li, J. Liu, X. Lai, X. Yu, X. Chen, H. Fu, J. Hu, *Mater. Lett.,* **2013,** *93,* 278-281.
[72] Y. Wang, H. Arandiyan, S.A. Bartlett, A. Trunschke, H. Sun, J. Scott, A.F. Lee, K. Wilson, T. Maschmeyer, R. Schlögl, R. Amal, *Appl. Catal. B: Environ,* **2020,** *277,* 119029.
[73] J. Georgieva, E. Valova, I. Mintsouli, S. Sotiropoulos, D. Tatchev, S. Armyanov, A. Hubin, J. Dille, A. Hoell, V. Raghuwanshi, N. Karanasios, L. Malet, *J. Electroanalytical Chem.*, **2015**, 754, 65-74.
[74] B. Vanrenterghem, A. Papaderakis, S. Sotiropoulos, D. Tsiplakides, S. Balomenou, S. Bals, T. Breugelmans, *Electrochimica Acta*, **2016**, 196, 756-768.
[75] A.H. Dam, H. Wang, R. Dehghan-Niri, X. Yu, J.C. Walmsley, A. Holmen, J. Yang, D. Chen, *ChemCatChem,* **2019,** *11,* 3401-3412.
[76] X. Di, G. Lafaye, C. Especel, F. Epron, J. Qi, C. Li, C. Liang, *ChemSusChem*, **2019**, *12*, 807-823.
[77] M.J. Taylor, S.K. Beaumont, M.J. Islam, S.Tsatos, C.A.M. Parlett, M.A. Issacs, G. Kyriakou, *Appl. Catal. B: Environ,* **2021,** *284,* 119737.
[78] L. Ruan, H. Zhang, M. Zhou, L. Zhua, A. Pei, J. Wang, K. Yang, C. Zhang, S. Xiao, B.H. Chen, *Molecular Catal.* **2020,** *480,* 110639.
[79] T. Yoshii, K. Nakatsuka, Y. Kuwahara, K. Mori, H. Yamashita, *RSC Adv.*, **2017**, *7*, 22294-22300.
[80] G. Zhou, Y. Dong, D. He, *Appl. Surf. Sc.,* **2018,** *456,* 1004-1013.
[81] A. Brenner, G.E. Riddel, *J. Res. Natl. Bur. Std.*, **1946**, 37, 31-34.
[82] F. Muench, *ChemElectroChem*, **2021**, *8*, 2993-3012.
[83] S. Szabo and F. Nagy, *J. Electroanal. Chem.*, **1976**, *70*, 357.
[84] M.C. Schoenmaker-Stolk, J.W.W. Verwijs, J.J.F. Schoelten, *Appl. Catal.*, **1987**, *30*, 339.
[85] S. Szabo, F. Nagy, *J. Electroanal. Chem*., **1977**, *84*, 93-98.
[86] S. Szabo, F. Nagy, *J. Electroanal. Chem.*, **1977**, *85*, 339-343
[87] S. Szabo, F. Nagy, *J. Electroanal. Chem*., **1978**, *87*, 261-265
[88] S. Szabo, F. Nagy, *J. Electroanal. Chem.*, **1984**, *160*, 299-303.
[89] S. Szabo, F. Nagy, *J. Electroanal. Chem.*, **1987**, *230*, 233-240.
[90] S. Szabo, I. Bakos, F. Nagy, *J. Electroanal. Chem.*, **1989**, *271*, 269-277.
[91] I. Bakos, S. Szabo and F. Nagy, T. Mallat and Z. Bodnar, *Electroanal. Chem.*, **1991**, *309*, 293-301.
[92] Z. Bodnar, T. Mallat, I. Bakos, S. Szabo, Z. Zsoldos, Z. Schay, *Appl. Catal. A*, **1993**, *102*, 105-123.
[93] S. Szabo, F. Nagy, *Isr. J. Chem.*, **1979**, *18*, 162-165.
[94] J.C. Menezo, M.F. Denanot, S. Peyrovi, J. Barbier, *Appl. Catal*., **1985**, *15*, 353-356.
[95] C.L. Pieck, P. Marecot, J. Barbier, *Appl. Catal. A*, **1996**, *134*, 319-329.
[96] S. Szabo, I. Bakos, *React. Kinet. Catal. Lett.*, **1998**, *65*, 259-263.
[97] R. Bachir, E. Lafitte, P. Marecot, B. Didillon, J. Barbier, *J. Chim. Phys.*, **1997**, *94*, 1906-1913.
[98] R. Bachir, P. Marecot, B. Didillon, J. Barbier, *Appl. Catal. A*, **1997**, *164*, 313-322.
[99] G. Del Angel, R. Melendrez, V. Bertin, J.M. Dominguez, P. Marecot, J. Barbier, *Stud. Surf. Sci. Catal.*, **1993**, *78*, 171.
[100] V. Bertin, P. Bosch, G. Del Angel, R. Gomez, J. Barbier, P. Marecot, *J. Chim. Phys*., **1995**, *92*, 120-33.
[101] P. Del Angel, J.M. Dominguez, G. Del Angel, J.A. Montoya, E. Lamy-Pitara, S. Labruquere, J. Barbier, *Langmuir*, **2000**, *16*, 7210-7217.
[102] J.M. Dumas, S. Rmili, J. Barbier, *J. Chim. Phys.*, **1998**, *95*, 1650-1665.
[103] R. Melendrez, G. Del Angel, V. Bertin, M.A. Valenzuela, J. Barbier, *J. Mol. Catal. A*, **2000**, *157*, 143-149.
[104] G. Espinosa, G. Del Angel, J. Barbier, P. Bosch, V. Lara, D. Acosta, *J. Mol. Catal. A*, **2000**, *164*, 253-262.
[105] C. Montassier, J.C. Menezo, J. Moukolo, J. Naja, L.C. Hoang, J. Barbier, J.P. Boitiaux, *J. Mol. Catal.*, **1991**, *70*, 65-84.
[106] J.C. Menezo, L.C. Hoang, C. Montassier, J. Barbier, *React. Kinet. Catal. Lett.*, **1992**, *46*, 1-6.

[107] C.L. Pieck, P. Marecot, J. Barbier, *Appl. Catal. A*, **1996**, *141*, 229-244.
[108] C.L. Pieck, P. Marecot, J. Barbier, *Appl. Catal. A*, **1996**, *143*, 283-298
[109] C.L. Pieck, P. Marecot, J. Barbier, *Appl. Catal. A*, **1996**, *145*, 323-334.
[110] J. Barbier, P. Marecot, C.L. Pieck, *Stud. Surf. Sci. Catal.*, **1997**, *111*, 327-334.
[111] C.L. Pieck, P. Marecot, C.A. Querini, J.M. Parera, J. Barbier, *Appl. Catal. A*, **1995**, *133*, 281-292.
[112] F. Epron, F. Gauthard, C. Pineda, J. Barbier, *J. Catal.*, **2001**, *198*, 309-318.
[113] F. Epron, F. Gauthard, J. Barbier, *Appl. Catal. A*, **2002**, *237*, 253-261
[114] F. Gauthard, F. Epron, J. Barbier, *J. Catal.*, **2003**, *220*, 182-191.
[115] P. Samoila, M. Boutzeloit, C. Especel, F. Epron, P. Marécot, *Appl. Catal.* A, **2009**, *369*, 104-112.
[116] P. Samoila, M. Boutzeloit, C. Especel, F. Epron, P. Marécot, *J. Catal.*, **2010**, *276*, 237-248
[117] A. Le Valant, S. Bouchet, A. Van Assche, C. Especel, F. Epron, *J. Catal*., **2021**, *397*, 64-74.
[118] T. Ekou, A. Vicente, G. Lafaye, C. Especel, P. Marecot, *Appl. Catal. A*, **2006**, *314*, 64-72.
[119] T. Ekou, A. Vicente, G. Lafaye, C. Especel, P. Marecot, *Appl. Catal. A*, **2006**, *314*, 73-80.
[120] G. Corro, P. Marecot, J. Barbier, *Stud. Surf. Sci. Catal.*, **1997**, *111*, 359-366.
[121] C. Carnevillier, F. Epron, P. Marecot, *Appl. Catal. A*, **2004**, *275*, 25-33.
[122] F. Epron, C. Carnevillier, P. Marecot, *Appl. Catal. A*, **2005**, *40*, 157-169.
[123] G. Espinosa, G. Del angel, J. Barbier, P. Marecot, I. Schifter, *Stud. Surf. Sci. Catal.*, **1997**, *111*, 421-426.
[124] J. Sa, S. Gross, H. Vinek, *Appl. Catal. A*, **2005**, *294*, 226-234.
[125] J. Sa, H. Vinek, *Appl. Catal. B*, **2005**, *57*, 247-256.
[126] B. Nohair, C. Especel, P. Marecot, C. Montassier, L.C. Hoang, J. Barbier, *C.R. Chimie*, **2004**, *7*, 113-118.
[127] B. Nohair, C. Especel, G. Lafaye, P. Marecot, L.C. Hoang, J. Barbier, *J. Mol. Catal. A*, **2005**, *229*, 117-126.
[128] A. Garron, K. Lazar, F. Epron, *Appl. Catal. B*, **2005**, *57*, 57-69.
[129] D.P. Barbosa, P. Tchiéta, M. do C. Rangel, F. Epron, *J. Mol. Catal. A*, **2013**, *366*, 294-302.
[130] B. Tapin, F. Epron, C. Especel, B.K. Ly, C. Pinel, M. Besson, *Catal. Today*, **2014**, *235*, 127-133.
[131] B.K. Ly, B. Tapin, F. Epron, C. Pinel, C. Especel, M. Besson, *Catal. Today*, **2020**, *355*, 75-83.
[132] B. Tapin, B.K. Ly, C. Canaff, F. Epron, C. Pinel, M. Besson, C. Especel, *Mater. Chem. Phys.*, **2020**, *252*, 123225.
[133] J.M. Dumas, C. Geron, H. Hadrane, P. Marecot, J. Barbier, *J. Mol. Catal.*, **1992**, *77*, 87-98.
[134] G. Lafaye, C. Micheaud-Especel, C. Montassier, P. Marecot, *Appl. Catal. A*, **2002**, *230*, 19-30.
[135] G. Lafaye, T. Ekou, C. Micheaud-Especel, C. Montassier, P. Marecot, *Appl. Catal. A*, **2004**, *257*, 107-117.
[136] G. Lafaye, C. Mihut, C. Especel, P. Marecot, M. Amiridis, *Langmuir*, **2004**, *20(24)*, 10612-10616.
[137] A. Vicente, T. Ekou, G. Lafaye, C. Especel, P. Marécot, C.T. Williams, *J. Catal.*, **2010**, *275*, 202-210.
[138] M. Boutzeloit, V.M. Benitez, C. Especel, F. Epron, C.R. Vera, C.L. Pieck, P. Marecot, *Catal. Commun.*, **2006**, *7*, 627-632.
[139] P. Samoila, M. Boutzeloit, V. Benitez, S.A. D'Ippolito, C. Especel, F. Epron, C.R. Vera, P. Marécot, C.L. Pieck, *Appl. Catal. A,* **2007**, 37-45.
[140] V. Benitez, M. Boutzeloit, V.A. Mazzieri, C. Especel, F. Epron, C.R. Vera, P. Marécot, C.L. Pieck, *Appl. Catal. A,* 319, **2007**, 210-217.
[141] S.A. D'Ippolito, C.R. Vera, F. Epron, C. Especel, P. Marécot, C.L. Pieck, *Catal. Today*, **2008**, *133–135*, 13-19.
[142] S.A. D'Ippolito, C. Especel, F. Epron, P. Marécot, C.L. Pieck, *Appl. Catal. A,* **2010***, 388,* 272-277.
[143] S.A. D'Ippolito, C.R. Vera, F. Epron, P. Samoila, C. Especel, P. Marécot, L.B. Gutierrez, C.L. Pieck, *Appl. Catal. A,* **2009***, 370,* 34-41.
[144] A. Garron, K. Lazar, F. Epron, *Appl. Catal. B*, **2006**, *65*, 240-248.
[145] S. Escribano, R. Mosdale, P. Marecot, P. Korovtchenko, G. Lafaye, J. Barbier, "CO tolerance of multi-metallic platinum based catalysts", Proceedings "France -Deutschland Fuel Cell Conference 2002", oct 7-10, p10, Forbach (2002).
[146] A. Furcht, A. Tungler, S. Szabo, A. Sarkany, *Appl. Catal. A*, **2002**, *226*, 155-161.
[147] A. Furcht, A. Tungler, S. Szabo, Z. Schay, L. Vida, I. Gresits, *Appl. Catal. A*, **2002**, *231*, 151-157.
[148] S.S. Djokic, in Modern Aspects of Electrochemistry, B.E. Conway and R.E. White Ed. (Kluver Academic/Plenum Publishers, 2002), Vol.35, pp. 51-133.
[149] S.S. Djokic, P.L. Cavallotti, in Electroless deposition: theory and applications, S.S. Djokic Ed. (Springer, 2010) Vol 48pp. 251-289
[150] K.D. Beard, M.T. Schaal, J.W. Van Zee, J.R. Monnier, *Appl. Catal. B*, **2007**, *72*, 262-271.

[151] C.J. Zhong, J.R. Regalbuto, in Comprehensive Inorganic Chemistry II, K. Poeppelmeier, Ed. (Elsevier, ed. 2, 2013), pp. 75-102.
[152] J.E.A.M. Van Den Meeracker, *J. Appl. Electrochem.,* **1981**, *11*, 395-400.
[153] Bing Li, Ning Li, Deyu Li, Yanqing Wang, *J. Electrochem. Soc*., **2016**, *163*, D256.
[154] H. Kasimierczak, A. Wierzbicka-Miernik, I. Kwiecien, M.J. Szczerba, A. Korneva, M. Mosialek, K. Miernik, J. Wojewoda-Budka, *Electrochem. Acta*, **2019**, *303*, 157-165.
[155] T. Stohr, J. Brötz, M. Oezaslan, F. Muench, *Chem. Eur. J.,* **2020**, *26*, 3030-3033.
[156] Y. Ma, W. Li, E.C. Cho, Z. Li, T. Yu, J. Zeng, Z. Xie, Y. Xia, *ACS Nano*, **2010**, *4*, 6725-6734.
[157] M.T. Schaal, A.Y. Metcalf, J.H. Montoya, J.P. Wilkinson, C.C. Stork, C.T. Williams, J.R. Monnier, *Catal. Today*, **2007**, *123*, 142-150.
[158] J. Rebelli, A.A. Rodriguez, S.G. Ma, C.T. Williams, J.R. Monnier, *Catal. Today*, **2011**, *160*, 17-178.
[159] K.D. Beard, D. Borelli, A.M. Cramer, D. Blom, J.W. Van Zee, J.R. Monnier, *ACS Nano*, **2009**, *3*, 2841-2853.
[160] A.A. Rodriguez, C.T. Williams, J.R. Monnier, *Appl. Catal. A*, **2014**, *475*, 161-168.
[161] M.T. Schaal, A.C. Pickerel, C.T. Williams, J.R. Monnier, *J. Catal*, **2008**, *254*, 131-143.
[162] K.D. Beard, J.W. Van Zee, J.R. Monnier, *Appl. Catal. B*, **2009**, *88*, 185-193.
[163] J. Rebelli, M. Detwiler, S.G. Ma, C.T. Williams, J.R. Monnier, *J. Catal*, **2010**, *270*, 224-233.
[164] W.J. Diao, J.M.M. Tengco, J.R. Regalbuto, J.R. Monnier, *ACS Catal.,* **2015**, *5*, 5123-5134.
[165] B.T. Egelske, J.M. Keels, J.R. Monnier, J.R. Regalbuto, *J. Catal*., **2020**, *381*, 374-384.
[166] G.L. Tate, B.A.T. Mehrabadi, W. Xiong, A. Kenvin, J.R. Monnier, *Nanomaterials*, **2021**, *11*, 793.
[167] A. Wongkaew, Y. Zhang, J. Myenard, M. Tengco, D.A. Blom, P. Sivasubramanian, P.T. Fanson, J.R. Regalbuto, J.R. Monnier, *Appl. Catal. B*, **2016**, *188*, 367-375.
[168] Q. Fu, H. Satlsburg, M. Flytzani-Stephnopoulos, *Science*, **2003**, 301, 935-938.
[169] J. Guzman, B.C. Gates, *J. Catal.*, **2004**, 226, 111-119.
[170] B. Qiao, A. Wang, X. Yang, L.F. Allard, Z. Jiang, Y. Cui, J. Liu, J. Li, T. Zhang, *Nat. Chem.*, **2011**, *3*, 634-641.
[171] X. Cui, W. Li, P. Ryabchuck, K. Junge, M. Beller, *Nat. Catal.,* **2018**, *1*, 385-397.
[172] X. Li, X. Yang, Y. Huang, T. Zhang, B. Liu, *Adv. Mater.*, **2019**, *31*, 1902031.
[173] M.B. Boucher, B. Zugic, G. Cladars, J. Kammert, M.D. Marcinkowski, T.J. Lawton, E.C.H. Sykes, M. Flytzani-Stephnopoulos, *Phys. Chem. Chem. Phys*., **2013**, *15*, 12187-12196.
[174] G. Sun, Z.J. Zhao, R. Mu, S. Zha, L. Li, S. Chen, K. Zang, J. Luo, Z. Li, S.C. Purdy, A.J. Kropf, J.T. Miller, L. Zeng, J. Gong, *Nat. Comm.,* **2018**, *9*, 4454.
[175] R.T. Hannagan, G. Giannakakis, M. Flytzani-Stephanopoulos, E.C.H. Sykes, *Chem. Rev.*, **2020**, *120*, 12044-12088.
[176] M.B. Boucher, B. Zugic, G. Cladaras, J. Kammert, M.D. Marcinkowski, T.J. Lawton, E.C.H. Sykes, M. Flytzani-Stephanopoulos, *Phys. Chem. Chem. Phys.,* **2013**,*15*, 12187-12196.